DESIGN OF ATTITUDE ESTIMATION ALGORITHMS FOR INERTIAL SENSORS ONLY MEASUREMENT SCENARIOS

A THESIS SUBMITTED TO
THE GRADUATE SCHOOL OF NATURAL AND APPLIED SCIENCES
OF
MIDDLE EAST TECHNICAL UNIVERSITY

BY

BATU CANDAN

IN PARTIAL FULFILLMENT OF THE REQUIREMENTS
FOR
THE DEGREE OF MASTER OF SCIENCE
IN
AEROSPACE ENGINEERING

MARCH 2022

Approval of the thesis:

DESIGN OF ATTITUDE ESTIMATION ALGORITHMS FOR INERTIAL SENSORS ONLY MEASUREMENT SCENARIOS

submitted by **BATU CANDAN** in partial fulfillment of the requirements for the degree of **Master of Science in Aerospace Engineering Department, Middle East Technical University** by,

Prof. Dr. Halil Kalıpçılar
Dean, Graduate School of **Natural and Applied Sciences** _____

Prof. Dr. Serkan Özgen
Head of Department, **Aerospace Engineering** _____

Assist. Prof. Dr. Halil Ersin Soken
Supervisor, **Aerospace Engineering, METU** _____

Examining Committee Members:

Prof. Dr. Ozan Tekinalp
Aerospace Engineering, METU _____

Assist. Prof. Dr. Halil Ersin Soken
Aerospace Engineering, METU _____

Prof. Dr. Cengiz Hacızade
Aeronautical Engineering, Istanbul Technical University _____

Prof. Dr. Umut Örgüner
Electrical and Electronics Engineering, METU _____

Assist. Prof. Dr. Ali Türker Kutay
Aerospace Engineering, METU _____

Date: 24.03.2022

I hereby declare that all information in this document has been obtained and presented in accordance with academic rules and ethical conduct. I also declare that, as required by these rules and conduct, I have fully cited and referenced all material and results that are not original to this work.

Name, Surname: Batu Candan

Signature :

ABSTRACT

DESIGN OF ATTITUDE ESTIMATION ALGORITHMS FOR INERTIAL SENSORS ONLY MEASUREMENT SCENARIOS

Candan, Batu
M.S., Department of Aerospace Engineering
Supervisor: Assist. Prof. Dr. Halil Ersin Soken

March 2022, 81 pages

This thesis proposes four novel robust Kalman filter algorithms for attitude estimation using only the measurements of an inertial measurement unit. Efficiency and optimality of the Kalman filter based attitude filters are correlated with appropriate tuning of the covariance matrices. Manual tuning process is a difficult and time-consuming task. Specifically, the inertial measurement unit-only attitude estimation filters are prone to the external accelerations unless their covariances are adapted to gain robustness. The proposed algorithms provide an adaptive method for tuning the measurement noise covariance such that they can accurately estimate the attitude. The proposed methodologies are tested and compared with other filtering algorithms in the literature under different dynamical conditions and using real-world experimental datasets in order to validate their effectiveness. Results show that in highly dynamic scenarios especially the multiple tuning factor strategy can increase the attitude estimation accuracy more than two-times compared to the competitive algorithms.

Keywords: Attitude estimation, covariance tuning, robust Kalman filter

ÖZ

SADECE ATALETSEL SENSÖR ÖLÇÜM SENARYOLARI İÇİN YÖNELİM TAHMİNİ ALGORİTMALARININ TASARIMI

Candan, Batu
Yüksek Lisans, Havacılık ve Uzay Mühendisliği Bölümü
Tez Yöneticisi: Dr. Öğr. Üyesi Halil Ersin Söken

Mart 2022 , 81 sayfa

Bu tez, yalnızca bir ataletsel ölçüm biriminin ölçümlerini kullanarak yönelim tahmini için dört yeni gürbüz Kalman filtresi algoritması önermektedir. Kalman filtresi tabanlı yönelim filtrelerinin verimliliği ve optimalliği, kovaryans matrislerinin uygun şekilde ayarlanması ile ilişkilidir. Manuel ayar işlemi zor ve zaman alıcı bir iştir. Spesifik olarak, yalnızca ataletsel ölçüm birimi tabanlı yönelim tahmini filtreleri, kovaryansları gürbüzlük kazanmak üzere uyarlanmadıkça dış ivmelere karşı savunmasızdır. Önerilen algoritmalar, yönelimin doğru bir şekilde tahmin edebileceği uyarlanabilir bir yöntem ortaya koymaktadır. Önerilen metodolojiler, etkinliklerini doğrulamak için farklı dinamik koşullar altında ve gerçek dünya deneysel veri kümeleri kullanılarak literatürdeki diğer mevcut filtreleme algoritmaları ile karşılaştırılmıştır. Sonuçlar, dinamik senaryolarda, özellikle çoklu ayar faktörü stratejisinin, rakip algoritmalara kıyasla yönelim tahmini doğruluğunu iki kattan fazla artırabildiğini göstermektedir.

Anahtar Kelimeler: Yönelim tahmini, kovaryans ayarlama, gürbüz Kalman filtresi

Dedicated To My Dear Family and Loved Ones

ACKNOWLEDGMENTS

First of all, I would like to express my deepest gratitude to my supervisor, Asst. Prof. Dr. Halil Ersin Soken for his endless support, interest and encouragements throughout my study. It was such a miraculous chance to meet with him two and a half years ago for me who was just a naive, fresh graduate from undergrad. I am grateful to him for his precise guidance that leads my career path.

I would like to thank my father Can Candan, my dear brother Ege Candan but especially my dear mother Sevgi Candan, without her I cannot be in the place where I currently am, for their support, encouragements and good wishes.

I would like to thank a special person, a beloved one who is always supporting me, giving me a will to struggle and proving her love is my "wonderwall" during the creation of this study. Without any hesitations, let the mankind and history witness that it is my promise trying to make You the happiest woman in the Earth and I will always shout "Omnia Vincit Amor: Et Nos Cedamus Amori" as Publius Virgil did.

I would like to extend my acknowledgments to my dear friends from my undergrad and grad years, my colleagues from Roketsan Missiles Inc. and 5^{th} Main Maintenance Center for their friendship and support.

Finally, I would like to thank my dear mentor Dr. Robert Fonod and Dr. Nitin J. Sanket from University of Maryland for his inspirational website and visual usage permissions.

TABLE OF CONTENTS

LIST OF TABLES

TABLES

LIST OF FIGURES

FIGURES

LIST OF ABBREVIATIONS

2D	2 Dimensional
3D	3 Dimensional
6D	6 Dimensional
6-DoF	Six Degrees of Freedom
AI	Artificial Intelligence
ARW	Angular Random Walk
CF	Complementary Filter
CKF	Cubature Kalman Filter
DCM	Direction Cosine Matrix
ECEF	Earth-Centered Earth-Fixed
ECI	Earth-Centered Inertial
EKF	Extended Kalman Filter
ENU	East-North-Up
ESOQ	Estimator of Optimal Quaternion
FKF	Fast Kalman Filter
FOAM	Fast Optimal Attitude Matrix
GNSS	Global Navigation Satellite System
GPS	Global Positioning System
HEAO	High Energy Astronomy Observatory
ICBM	Intercontinental Ballistic Missile
IGRF	International Geomagnetic Reference Field
IMU	Inertial Measurement Unit
INS	Inertial Navigation System
KF	Kalman Filter

K_i	Integral Gain
K_p	Proportional Gain
LEKF	Lightweight Quaternion-Based Extended Kalman Filter
MAGSAT	Magnetic Field Satellite
MARG	Magnetic, Angular Rate and Gravity
MAV	Micro Aerial Vehicle
MEKF	Multiplicative Extended Kalman Filter
MEMS	Micro-Electro-Mechanical Systems
MSF	Multiple-Scale Factor
MTF	Multiple-Tuning Factor
NASA	National Aeronautics and Space Administration
NED	North-East-Down
PI	Proportional-Integral
QUEST	Quaternion Estimator
RKF	Robust Kalman Filter
RMSE	Root Mean Square Error
SAGE	Defense Industries Research and Development Institute
SO(3)	Special Orthogonal Group
SSF	Single-Scale Factor
STF	Single-Tuning Factor
SVD	Singular Value Decomposition
TUBITAK	The Scientific and Technological Research Council of Turkey
UAV	Unmanned Aerial Vehicle
UKF	Unscented Kalman Filter
VRW	Velocity Random Walk

CHAPTER 1

INTRODUCTION

Orientation estimation has been a significant problem for decades in various applications such as robotics, navigation, aerospace, motion tracking, positioning and localization of the objects. Over decades, the humanity relies on to use information from both internal and external sensors for determining the orientation and position information. The fusion of global navigation satellite system or global positioning system and inertial navigation system emerged from the need of accurate determination of position and orientation. Table 1.1 shows that these two systems complement each other's weakness and fusing their data can provide a complete solution in most cases [1].

Table 1.1: Important characteristics of INS and GNSS

Characteristics	INS	GNSS
Solution Accuracy	Nice short term accuracy, but deteriorates in prolonged scenarios	Nice long term accuracy with noisy sampling within short time period
Initial Condition Requirement	Yes	No
Attitude Information Availability	Available	Generally not available
Sensitive against Gravity	Yes	No
Self-Sufficient	Yes	No
Immune against Electronic Attacks	Yes	No
Output Sampling Rate	High	Low

As seen in Table 1.1, GNSS is sensitive against the external disturbances and threats such as jamming or spoofing. Moreover, implementing GPS receivers and antennae within the systems increases the costs of operation. This leads the scientists and researchers to seek for self-contained solutions that are able to provide the position and orientation information accurately using only internal sensor frameworks.

Inertial navigation system is such a framework composed of inertial sensors (accelerometers and gyroscopes). In order to estimate the orientation appropriately in all three axes, required sensor layout for all of these methods is usually a set of magnetic, angular rate and gravity sensors also known as attitude and heading reference systems. Especially, over the past two decades technological developments resulted in lightweight, economical, accurate magnetic and inertial measurement units. However, despite the latest improvements, it is important to emphasize each sensor exhibits some form of uncertain error characteristics so that numerous sensor fusion algorithms have appeared in literature [2].

Numerous applications such as the stability control of the land and aerial platforms, human balancing require only the attitude angles and not the heading, yaw angle since the accelerometer is not able to sense and extract the rotation about the yaw axis. If needed, yaw angle can be estimated in addition from the magnetometer measurements. Owing to the accessibility of small and cheap IMUs, today IMU-only attitude estimation has a diverse application field. IMUs are used for orientation estimation of not only robots, drones, cars and other autonomous vehicles that we can think of, but also in many other fields from motion capture for movies and gaming to ambulatory treatment [3]. Attitude information can be obtained in a straightforward way in the absence of any external acceleration via decomposing the gravity vector along the axes. However, the accelerometer measurements are usually disturbed by the external acceleration of the platform during the motion, prohibiting their use for accurate attitude estimation. Thus, our main aim is to provide an IMU-only two-dimensional attitude estimation method, which is robust against external accelerations and can be used in different applications without requiring extensive modification other than adapting to the actual problem and tuning.

Following survey is to light the way from the beginning of sensor orientation determination studies. A review is provided for the studies on accelerometer-gyroscope fusion for estimating the roll and pitch angles, commonly referred as the tilt angles that are two of the attitude states.

1.1 Literature Survey

The optimal algorithms for the attitude estimation problem using only INS or/and magnetometers have been developed for last fifty years and divided into three common groups, algebraic/static methods, KFs and CFs, respectively. First efforts to correctly estimate the attitude start to seek a solution for Wahba's problem, that is to search and find a rotation matrix between two different coordinate systems from vector observations [4]. In literature, solutions using pure algebra started to appear and some of the acknowledged methods are Davenport's q-Method [5], using quaternion algebra, Black's TRIAD [6], Shuster's QUEST algorithm [7], Markley's Singular Value Decomposition (SVD) method and Mortari's Estimators of the Optimal Quaternion algorithms (ESOQ1-2) [8]. Later, originated from the work of Rudolf E. Kalman [9], various algorithms have been proposed using this recursive method for estimating the attitude and the orientation of a system. In attitude estimation problems, KF-based methods focus on the accurate modeling of the external acceleration, disturbances and fine tuning of the noise covariance matrices with different approaches such as fuzzy, adaptive, and even manual tuning methods. All of these methods usually focus the accurate modelling of the measurement noise covariance. Neural network and fuzzy logic based applications [10, 11], adaptive algorithms [12, 13, 14], cascaded structures that include different but coupled KFs [15] and other methods that use unscented Kalman filtering and gradient-descent strategies [16, 17, 18] are proposed in literature for solving the attitude estimation problem. On the other hand, simpler and less complex CF methodology due to the frequency-based solution scheme, becomes another strategy developed for the attitude estimation problem. In [19, 20, 21, 22, 23], the attitude is evaluated via fusing the gyroscope and accelerometer readings in a complementary fashion. However, it is reported that the performance of common CFs deteriorates in prolonged and highly dynamic scenarios [24]. Nevertheless, Madgwick and Mahony filters [25, 26] are depicted as the benchmark algorithms in this study due to their popularity, ease of implementation in various applications and computational efficiency.

With advancing computational capacity, KFs and nonlinear Kalman filtering algorithms (e.g. EKF) are also being used in orientation estimation. They tend to behave better in terms of attitude estimation accuracy [27, 28]. In [29, 30, 31, 32, 33], EKF-based methods are used for solving the attitude estimation problem via focusing on accurate modeling of the external acceleration and fine tuning of the noise covariances with different approaches such as fuzzy, adaptive, and even manual tuning methods. In [34], authors represented the external acceleration as first-order low-pass filtered white noise process and altered the measurement noise covariance matrix during the dynamic conditions where the external accelerations present. At first look, this methodology seems to perform better when compared with benchmark algorithms, but it cannot sustain efficient estimation quality due to some fundamental reasons. First, the estimated external acceleration is assumed to be split equally in all the axes, which is not the general case in practice. Second, the filter gain cannot correct the predictions optimally since the modelled external acceleration process is low pass filtered with the same cutoff constant all along the motion. Therefore, it can be stated that the accurate filter gain adaptation and the compensation of external acceleration become very important. The general trend behind these methods is the appropriate adjustment of measurement noise covariance which is related with the accurate compensation of external accelerations and disturbances. In [24], cascaded filtering structure is proposed, that is similar to the one proposed in [15], but does not need to rely on any external sensor framework. Including two different, but coupled KFs, for both the attitude and gyro bias estimation, measurement noise covariance matrix is tuned via weighting matrix and adaptive cutoff constant strategy for improving the attitude estimation quality is incorporated. Another strategy in the literature is to adapt the measurement noise covariance matrix via introducing fuzzy-logic adaptations as in [35] and [36]. Recent studies have shown that the ellipsoidal method [37] and UKF [38] can be also used for estimating the attitude of different systems. However, it should be noted that while there is an increasing trend for having more accurate solutions with complex algorithms, computational load becomes one of the crucial drawbacks.

1.2 Contribution of the Thesis

This thesis study proposes four different RKF algorithms for estimating the two-axis attitude (i.e., roll and pitch angles) using the measurements of only an IMU. The proposed methods addresses the covariance uncertainty due to the external accelerations via adaptively scaling and tuning the measurement noise covariance matrix, while keeping the estimation algorithm in the KF framework. In contrast to the existing literature, both algorithms incorporate a straightforward adaptation method, which has almost no extra computational demand and is easy to apply. Rather than using an approximate value for the covariance as in [34], the statistics are more accurately represented with the adaptively scaled and tuned covariance. A similar covariance tuning method given in [39, 40] scales the whole covariance matrix, whenever a measurement fault is detected.

In this work, apart from these studies, the scaling methodology is applied into the attitude estimation problem and the filter gain is adapted, when an external acceleration is detected, rather by estimating an additional covariance due to the external accelerations. Two different approaches for the two different RKF schemes differ by the number of scaling and tuning factors used for covariance adaptation. In scaling perspective, the measurement noise covariance matrix is to be scaled as whole by SSF and MSF respectively in line with the method given in [41]. In tuning perspective, first, the measurement noise covariance matrix is split into two parts, and a STF is introduced for tuning one part of measurement noise covariance matrix that is accounting for the external accelerations in line with the method given in [42]. However, even though showing enhanced performance, the scalar tuning process is not efficient enough due to the use of single scalar which adapts all measurement channels, simultaneously. The second approach adapts the same part of the covariance matrix via introducing MTFs to compensate the external accelerations more efficiently [43]. MTF approach mitigates the drawbacks of STF methodology since it is able to tune each measurement channels of the sensors, separately, during the motion. Both approaches are evaluated using the datasets for a micro aerial vehicle provided by [44] and [45], and the results are compared with a bunch of benchmark algorithms.

Main contribution of this thesis study is to introduce four different robust-adaptive approaches via scaling and tuning the measurement noise covariance matrix in KF structure and compensating the external accelerations efficiently in an adaptive way. Developed methodologies can be used in wide range of applications from pedestrian localization/navigation with limb-mounted or phone-integrated IMUs to unmanned platform navigation under the absence of external sensors such as visual-based sensors or GPS where the navigation and localization are able to be executed with only IMU sensor measurements.

1.3 The Outline of the Thesis

Organization of the paper is basically to give a brief theoretical background and preliminaries for the attitude estimation problem in Section II. In Section III, the different branches of the attitude estimation methodologies are given with a bunch of benchmark methods used for the performance comparison and evaluation in the next section. Finally, in Section IV, the proposed methods including two different strategies with two different approaches of the proposed RKF algorithms are given. Section V gives the evaluation and comparison of the performance for the proposed algorithms and the benchmarks methods selected from the recent literature. Last section, Section VI concludes the article with further discussions and future work opportunities with the extend of the scope of this thesis study.

CHAPTER 2

PRELIMINARIES

2.1 Coordinate Frames

In this section, the coordinate systems and attitude representation preference that are used in the context of this thesis are to be given. Four different coordinate systems are used to define and represent the attitude, velocity and the position of the vehicle.

2.1.1 Earth-Centered Inertial Frame

As indicated by Sir Isaac Newton, ECI frame is a non-rotating and non-accelerating frame with its origin at the center of the Earth with respect to the fixed and distant stars. The x-axis points in the vernal equinox direction, while the z-axis points in the direction of the geographical North Pole and y-axis lies in the equatorial plane, ensuring the right-hand rule. In this study, the ECI frame is denoted simply by ‘I’ and to be called as "inertial frame".

2.1.2 Earth-Centered Earth-Fixed Frame

ECEF coordinate frame is somewhat similar to the inertial frame since they share the same origin. However, unlike inertial frame, ECEF frame rotates along with the Earth. The x-axis goes through the intersection of equatorial plane and the Greenwich meridian, while the z-axis points in the direction of the geographical North Pole as in ECI and y-axis lies in the equatorial plane, ensuring the right-hand rule. Figure 2.1 summarizes the illustration of ECI and ECEF coordinate frames [1].

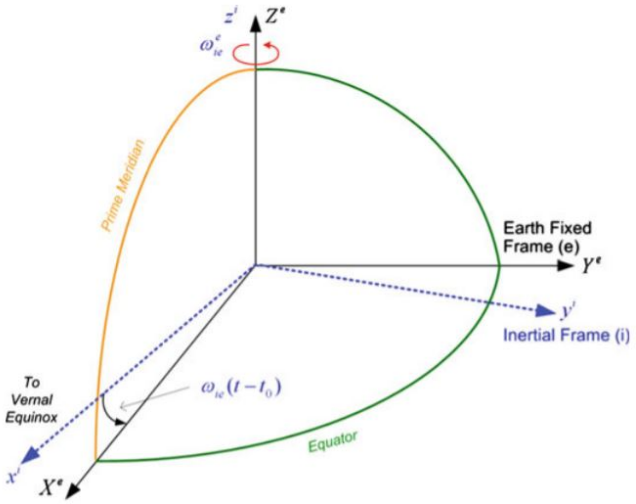

Figure 2.1: A demonstration of the ECI and ECEF coordinate frames

2.1.3 Navigation (Local-Level) Frame

As known as local geodetic frame or local-level frame, the navigation frame is used for indicating the system's attitude and position on or near to the surface of the Earth. Different representation for local-level frame can be made such as NED frame, East-North-Up frame. Figure 2.2 shows the ENU navigation frame in relation with ECI and ECEF frames. Note that x-axis points toward to east while y-axis points to the true north and z-axis completes the right-handed triad [1].

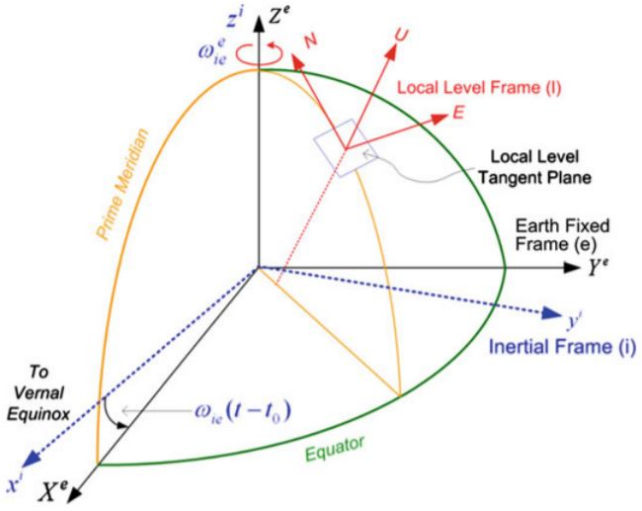

Figure 2.2: ENU navigation frame in relation to the ECI and ECEF frames

2.1.4 Wander Frame

Navigation frame includes a subtle detail that higher rotation rates about the z-axis are required in order to maintain the orientation of the navigation frame in the polar regions of the Earth (higher latitudes) than near the equator (lower latitudes), since the y-axis always points towards to the true north. So, as can be seen on Figure 2.3b, when moving towards to the pole, reaching its maximum when it crosses the north pole, the navigation frame must rotate at higher rates to maintain its orientation. If the navigation frame passes over the pole, rotation rate can be infinite resulting in singularities. The wander frame eliminates the singularity problems via instead of always pointing northward, it rotates about z-axis with respect to the navigation frame. Figure 2.3 demonstrates the wander frame and its relation with the navigation frame. Note that the y-axis rotates by an angle α which is referred as "wander angle", anticlockwise from north, the z-axis is orthogonal to the reference ellipsoid pointing upward and x-axis completes the right-handed triad [1].

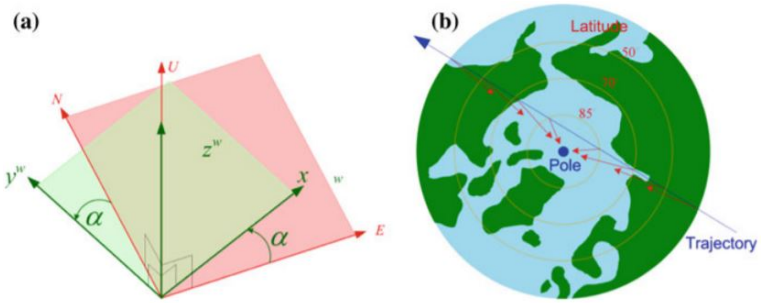

Figure 2.3: A demonstration of the wander frame in relation with the navigation frame

2.1.5 Body Frame

As known as "sensor frame" in most of the applications since the sensitive axes of inertial sensors usually are made to coincide with the axes of moving system that the sensors are deployed. Usually, the origin coincides with the center of gravity of the system while the y-axis points towards the front of the system, x-axis points towards transverse and the z-axis points towards vertical direction that is completing the right-handed triad [1].

However, it is possible to define different frame configurations similar as navigation frames. Figure 2.4 shows the body frame for a MAV platform.

Figure 2.4: A demonstration of the body frame for a MAV platform

2.2 Sensor Models

In this section of the thesis, inertial and magnetic sensors being considered/used in this study and the models governing their measurement characteristics are to be given. It is important to emphasize that in practice each sensor exhibits not only constant bias offset, but also varying bias errors, which are not accounted in the given models. Assuming that the sensor signals are stabilized after a few minutes of warm-up, the effect of varying biases can be neglected. So, in line with [34], the proposed algorithm does not take inertial sensor biases into account.

2.2.1 Gyroscope Model

Gyroscopes (shortly gyros) are the sensors that are able to measure angular rotation rates w.r.t. an inertial frame. They can output either angular rate or angles themselves depending on what types of gyro are used in practice [1]. Today, gyroscopes can be classified as mechanical, optical and microelectromechanical systems gyros. Measurement signals from the gyroscope ($\mathbf{y}_G$) can be modelled as following,

$$\mathbf{y_G} = {}^S\boldsymbol{\omega} + \mathbf{b}_G + \mathbf{S}_G{}^S\boldsymbol{\omega} + \mathbf{N}_G{}^S\boldsymbol{\omega} + \boldsymbol{n}_G. \tag{2.1}$$

${}^{S}\boldsymbol{\omega}$ and $\boldsymbol{n}_G$ are the actual angular rates and the gyroscope noise assumed to be uncorrelated, zero-mean white Gaussian noise characterized by $E[\boldsymbol{n}_G\boldsymbol{n}_G^T] = \sigma_G^2\mathbf{I}_3$ where σ_G^2 is the variance of gyro noise assumed to be split same along all axes. Other terms to be neglected in this study are gyroscope bias vector $\boldsymbol{b}_G$, gyro scaling factor matrix $\mathbf{S}_G$ and the matrix representing the non-orthogonality effects of the gyro $\mathbf{N}_G$, respectively.

2.2.2 Accelerometer Model

Accelerometers are the devices that can measure specific translational acceleration w.r.t. the inertial reference frame along their sensitive axis and can be found in different forms such as pendulous mass, vibratory and MEMS accelerometers in this era [1]. Measurement signals from the accelerometer sensor ($\mathbf{y}_A$) can be modelled as following,

$$\mathbf{y_A} = {}^{S}\mathbf{a} + {}^{S}\mathbf{g} + \mathbf{b}_A + \mathbf{S}_1({}^{S}\mathbf{a} + {}^{S}\mathbf{g}) + \mathbf{S}_2({}^{S}\mathbf{a} + {}^{S}\mathbf{g})^2 + \mathbf{N}_A({}^{S}\mathbf{a} + {}^{S}\mathbf{g}) + \delta\mathbf{g} + \boldsymbol{n}_A. \quad (2.2)$$

${}^{S}\mathbf{a}$ and ${}^{S}\mathbf{g}$ are the actual external acceleration and the gravity vector resolved in the body frame, respectively. $\boldsymbol{n}_A$ is the accelerometer noise assumed to be uncorrelated, zero-mean white Gaussian noise characterized by $E[\boldsymbol{n}_A\boldsymbol{n}_A^T] = \sigma_A^2\mathbf{I}_3$ where σ_A^2 is the variance of accelerometer noise assumed to be split same along all axes. Other terms to be neglected in this study are accelerometer bias vector $\boldsymbol{b}_A$, accelerometer linear scaling factor matrix $\mathbf{S}_1$, accelerometer non-linear scaling factor matrix $\mathbf{S}_2$, the matrix representing the non-orthogonality effects of the accelerometer $\mathbf{N}_A$, and deviation from the true/theoretical gravity $\delta\mathbf{g}$ respectively. Moreover, in [34], external acceleration ($\mathbf{a_t}$) was modeled as a first-order low-pass filtered white noise process as following,

$$\mathbf{a}_t = c_{\mathbf{a}}\mathbf{a}_{t-1} + \boldsymbol{\varepsilon}_t, \quad (2.3)$$

where c_a is a dimensionless, determinator constant specified for the cutoff frequency and the value of this constant is varying between 0 and 1. Time-varying error during the acceleration process is represented by $\boldsymbol{\varepsilon}_t$ which is modeled as Gaussian white noise. Table 2.1 demonstrates the general performance comparison of inertial measurement sensors.

Table 2.1: Performance classification of inertial measurement units

Performance Indicators	Strategic Grade IMUs	Navigation Grade IMUs	Tactical Grade IMUs	Commercial Grade IMUs
Gyroscope Bias (°/h)	0.0001-0.01	<0.01	1-10	360
Gyroscope ARW ($°/\sqrt{h}$)	Negligible	0.002	0.05-0.02	>1
Accelerometer Bias (μg)	0.1-1	<100	100-1000	>1000
Positional Accuracy (km/h)	<0.1	2	20-40	>100
Application Area	Submarines, ICBMs	Mapping, Georeferencing	Short time ammunitions	Research, Low-Cost navigation solutions

Note that, in this study main focus is to be limited within the use of commercial grade inertial sensors.

2.2.3 Magnetometer Model

Used for measuring either the magnetic field direction or magnitude of the magnetic field, magnetometers become an important part of navigation solutions together with inertial sensors. In this sense, signals from three-axis magnetometer measurement can be modeled as following [46].

$$\mathbf{y_M} = (\mathbf{I_3} + \mathbf{D})^{-1}({}^{I}_{S}\mathbf{R}^{T}\mathbf{B_I} + \mathbf{b_M} + \boldsymbol{n}_M). \tag{2.4}$$

Here, $\mathbf{B_I}$ is the magnetic field vector in reference ECI frame. $\mathbf{b_M} = \begin{bmatrix} b_{M_x} & b_{M_y} & b_{M_z} \end{bmatrix}^T$ denotes the magnetic bias vector, ${}^{I}_{S}\mathbf{R}$ is the direction cosine matrix of the sensor frame with respect to the inertial frame to be explained with details in following subsection and $\mathbf{D}$ matrix is referred as "scaling matrix", representing the scaling, symmetrical soft iron and non-orthogonality effects. $\boldsymbol{n}_M$ is the magnetometer noise assumed to be uncorrelated, zero-mean white Gaussian noise characterized by $E[\boldsymbol{n}_M\boldsymbol{n}_M^T] = \sigma_M^2\mathbf{I}_3$ where σ_M^2 is the variance of magnetometer noise assumed to be split same along all axes. It is important to emphasize that $\mathbf{D}$ matrix is assumed to have symmetrical property (any non-symmetrical soft iron and misalignment errors are neglected) with six independent terms as following.

$$\mathbf{D} = \begin{bmatrix} D_{11} & D_{12} & D_{13} \\ D_{12} & D_{22} & D_{23} \\ D_{13} & D_{23} & D_{33} \end{bmatrix}. \tag{2.5}$$

2.3 Inertial and Magnetic Sensor Performance Characteristics and Errors

Errors for sensor measurements are given previously showing how each error will affect the measurement output mathematically. However, before to go a step further, error characteristics and how each error changes the nature of the easement physically are required to be investigated. First, all of the sensors' performance can be assessed with following general terms [1].

- **Repeatability** is the ability of a sensor to provide the same output when the repeated same input is given assuming other factors are constant. Variation between provided outputs over multiple samplings gives the idea about the sensor's repeatability.

- **Stability** is the ability of a sensor to provide the same output when the same, constant input is given on a period of time assuming other factors are constant. Variation between obtained output over single sampling gives the idea about the sensor's stability.

- **Drift** is the measure of change in output when the given input to the system is constant and is not changed.

These general terms are closely related with terms sensor scale factor, sensor bias, sensor noise and bandwidth that are to be discussed in following sub-section.

2.3.1 Inertial Sensor Errors

Inertial sensor errors are divided into two major categories named as systematic and random (stochastic) errors. While systematic errors are able to be compensated by laboratory or on-field calibration methods, random errors should be modelled stochastically for mitigating their negative consequences. These errors tend to appear in much more complex ways while the cost of the equipment is decreasing. Following, the most common errors observed on inertial sensors are to be investigated [1].

2.3.1.1 Offset Bias

Appeared both in accelerometers and gyroscopes, offset bias is independent from specific forces or angular rates to be measured and it can be defined by the shift from the true value when there is no input (zero input) even though the platform experiences no motion. These sensors' physical properties change resulting with different error characteristics over time and the sensor bias would increase depending on sensor usage and time. Figure 2.5 visually demonstrates this situation as following.

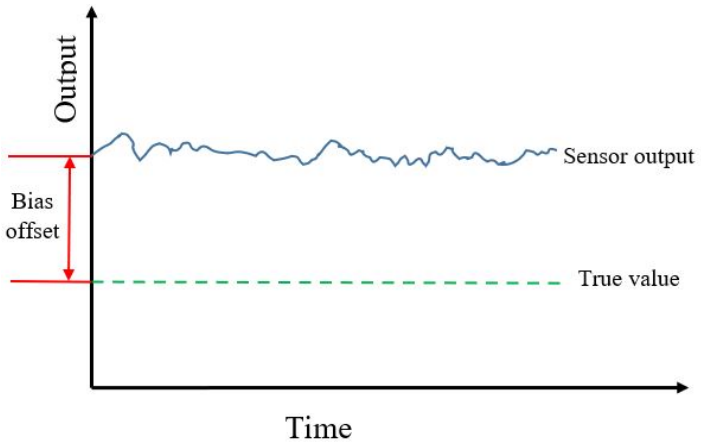

Figure 2.5: Visualization of the offset bias

2.3.1.2 Scale Factor and Sign Asymmetry

Appeared again both in accelerometers and gyroscopes, scale factor error is the shift of the input-output gradient from the unity. While the gyroscope scale factor error is associated with the true angular rate about the sensitive axis, accelerometer scale factor error is related with the true specific force along the sensitive axis. Figure 2.6 visually demonstrates this situation [1].

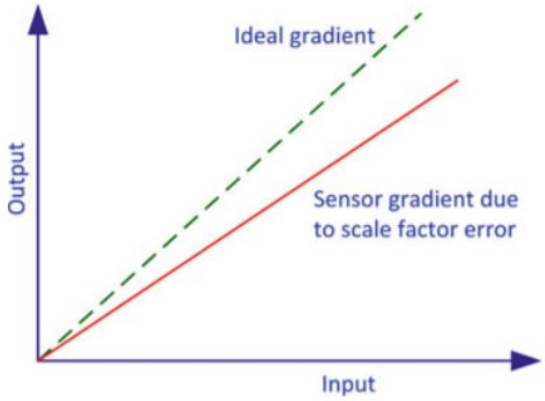

Figure 2.6: Visualization of the scale factor error

In some cases, scale factor error for given positive and negative inputs may differ. In this case, scale factor sign asymmetry is to appear and the situation would be like in Figure 2.7 [1].

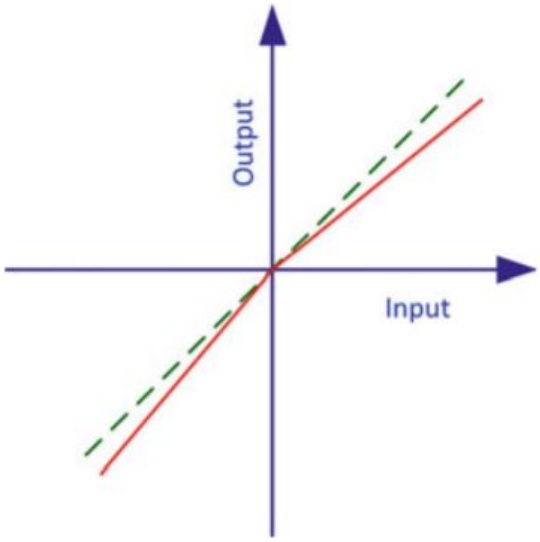

Figure 2.7: Visualization of the scale factor sign asymmetry error

2.3.1.3 Non-Linearity

As its name indicates, the non-linearity error is originated from the non-linearity between the input and the output and the situation can be seen in Figure 2.8 [1].

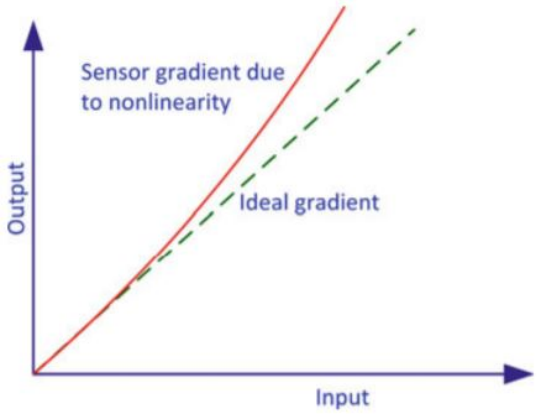

Figure 2.8: Visualization of the non-linearity error

2.3.1.4 Dead Zone

As seen in Figure 2.9, the dead zone error can be defined that the presence of unavailable output even though there is a related input on the system [1].

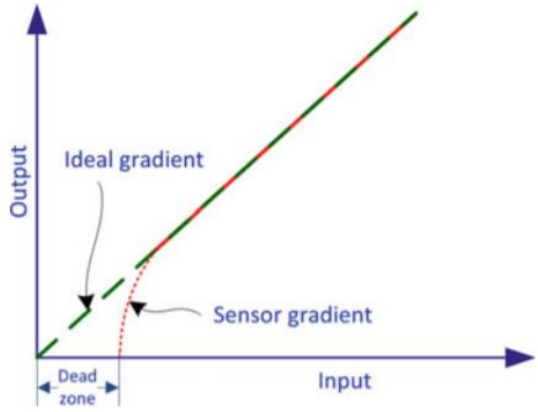

Figure 2.9: Visualization of the dead zone error

2.3.1.5 Quantization

If the digital systems use the inputs coming from analog machines that results with transmitting analog signals, the quantization error is observed in all digital systems as can be seen in Figure 2.10 [1].

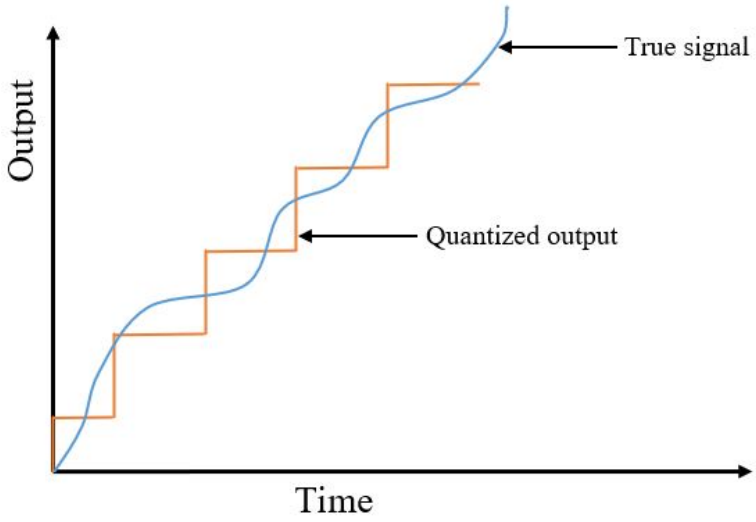

Figure 2.10: Visualization of the quantization error

2.3.1.6 Non-Orthogonality

As its name indicates, the non-orthogonality error is related with the break down of axes mutual orthogonality due to the manufacturing errors usually. Figure 2.11 demonstrates this error situation where θ_{zy} and θ_{zx} depict the angular offset from the planes.

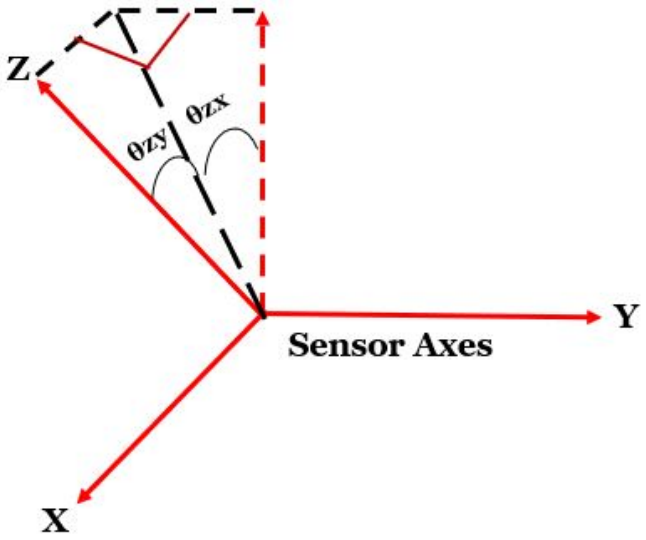

Figure 2.11: Visualization of the non-orthogonality error

2.3.1.7 Misalignment

Usually occur in cases when the sensitive axes of the inertial sensors are mounted with an offset with respect to the body frame. This imperfection is visible on Figure 2.12 in which $\delta\theta$ is the small angle offset between the axes due to the misalignment.

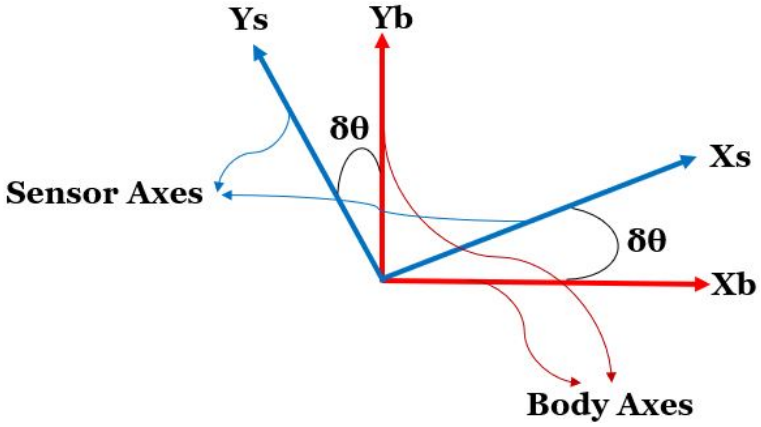

Figure 2.12: Visualization of the misalignment error

2.3.1.8 Run-to-Run Bias

Under the sub-group of the bias repeatability term, run-to-run bias is defined as the change in bias offset for each run time [1].

2.3.1.9 Bias Drift

Stochastic changes in the bias over the measurement period is classified under bias drift. In other words, it can be defined as the instability of the sensor bias during the run time. Whereas bias offset is deterministic, bias drift is random error seen in inertial sensors and it is usually dependent on the changes in temperature.

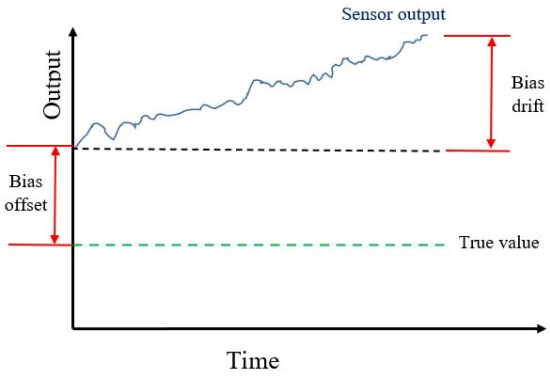

Figure 2.13: Visualization of the bias drift error

2.3.1.10 Scale Factor Instability

Usually due to the temperature variations on the working environment, there exist random changes in scale factor during a measurement session. This gives an idea about the repeatability of the sensor and is called as the scale factor instability or the run-to-run scale factor.

2.3.1.11 White Noise

Uncorrelated random signal set is called as white noise which is evenly distributed in whole frequency spectrum. Usually caused by power electronics or semiconductor devices within inertial sensors, effect of this phenomenon is visible in Figure 2.15 as following [1].

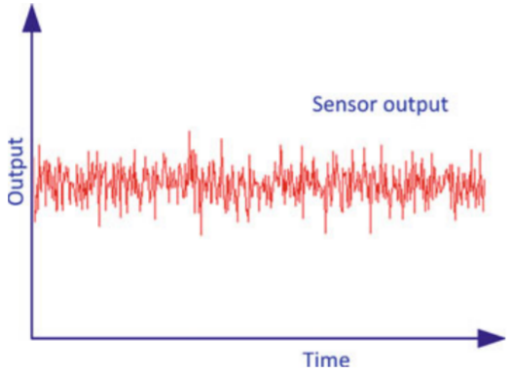

Figure 2.14: Visualization of the white noise error

2.3.2 Notes on Inertial Sensor Errors

Manufacturers of inertial sensors generally express the random errors and randomness via the "random walk" perspective. While velocity random walk is given for accelerometers with units of $\mu g/\sqrt{Hz}$ or $m/s/\sqrt{hr}$, angular random walk is given for gyroscopes with units of $deg/hr/\sqrt{Hz}$ or $deg/\sqrt{hr}$ as given on Figure 2.5 previously. These units indicate that while the one defines the randomness on inertial sensors, sampling frequency of the sensors and data acquisition systems is another important fact effecting the noise characteristics. This is closely related with the bandwidth (with unit Hz) of the sensors, defining the frequency interval that can be monitored via sensors, and the one should increase the bandwidth of the sensors for obtaining higher frequency data. However, while the monitoring process is facilitated by expanding the frequency interval, the measurements detected by the sensors would become much noisier [1].

2.3.3 Magnetic Sensor Errors

Three axis magnetometer (TAM) errors occur due to the internal, external error sources and inherent sensor errors. Briefly mentioned previously on magnetometer model section, now these errors can be listed with details as following.

2.3.3.1 Soft Iron Error

Materials that are generating magnetic fields in response to the external magnetic field sources are called as soft irons. Both magnitude and direction of the external field affect the generated field and the error originated from this phenomenon is called as soft iron bias. Note that since the orientation of the Earth's magnetic field with respect to the platform continuously changes for moving platforms, resulting soft iron errors are to be time-varying. Following, the soft iron error representation with 3×3 matrix $\mathbf{D}_{si}$ is shown [47, 48].

$$\mathbf{D}_{si} = \begin{bmatrix} \alpha_{xx} & \alpha_{xy} & \alpha_{xz} \\ \alpha_{yx} & \alpha_{yy} & \alpha_{yz} \\ \alpha_{zx} & \alpha_{zy} & \alpha_{zz} \end{bmatrix}, \tag{2.6}$$

where α_{ij} are the coefficients of soft iron effects which show the proportional relationship between the magnetic field applied to a soft iron and resulting induced magnetic field.

2.3.3.2 Hard Iron Error

Unlike soft irons, materials that have their own constant or slowly time-varying magnetic field (unwanted, interfering permanent magnetic fields) are called as hard irons, primarily composed from ferromagnetic materials, and the error to be originated from these materials is called as hard iron bias. This bias (denoted with $\mathbf{b}_{hi}$) is usually taken constant and must be subtracted for the sake of attitude determination process [48].

2.3.3.3 Null-Shift Error

In addition, there exists a null-shift error, denoted with $\mathbf{b}_{ns}$, due to the sensor imperfections which is adding a constant bias on the magnetometer measurements [48].

2.3.3.4 Magnetometer Scaling Error

Whereas the one expects the output of magnetometer triad is to be same from both sensitive axes, there might exist different sensitivity levels between axes and this difference should be taken account and represented via 3×3 matrix $\mathbf{D}_{sf}$ as following [48].

$$\mathbf{D}_{sf} = \begin{bmatrix} 1+\xi_x & 0 & 0 \\ 0 & 1+\xi_y & 0 \\ 0 & 0 & 1+\xi_z \end{bmatrix}, \tag{2.7}$$

Note that, ξ_x, ξ_y and ξ_z are the scale factors which might change over time due to the environmental effects and it needs to be emphasized they indicate the input-to-output sensitivity of each axis.

2.3.3.5 Magnetometer Non-Orthogonality Error

In case of the non-orthogonality between the sensors that are not orthogonal to each other, this error should be taken account to the measurements as a transformation of vector space basis. Denoted via 3×3 matrix $\mathbf{D}_{no}$, non-orthogonality is represented as following [48],

$$\mathbf{D}_{no} = \begin{bmatrix} 1 & 0 & 0 \\ \sin\rho & \cos\rho & 0 \\ \sin\phi\cos\lambda & \sin\lambda & \cos\phi\cos\lambda \end{bmatrix}, \tag{2.8}$$

where ρ, ϕ and λ are the angles between the y-sensor and y-axis, z-sensor and $y-z$ plane and the z-sensor and $y-z$ plane visually shown on Figure 2.16 as following.

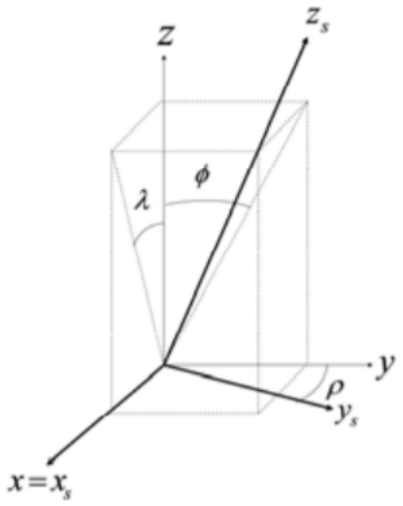

Figure 2.15: Visualization of the non-orthogonality error for magnetic sensors

2.3.3.6 Magnetometer Misalignment Error

Similar to the misalignment problem on inertial sensors due to the wrong mounting and imperfections, there exist errors caused by misalignment of magnetic sensors within body frame. Denoted via 3×3 matrix $\mathbf{D}_m$, misalignment is represented as following [48],

$$\mathbf{D}_m = \begin{bmatrix} 1 & -\varepsilon_z & \varepsilon_y \\ \varepsilon_z & 1 & -\varepsilon_x \\ -\varepsilon_y & \varepsilon_x & 1 \end{bmatrix}, \tag{2.9}$$

and note that the misalignment error matrix is defined with a skew-symmetric matrix composed from three small rotation angles ε_x, ε_y and ε_z.

2.3.4 Notes on Magnetic Sensor Errors

On Figure 2.17, errors that are originated from the internal/external disturbances are given in white boxes while the inherent sensors errors are given in dark gray boxes. In addition, errors that may be either inherent to sensor or originated from the disturbances are given with light gray boxes [48].

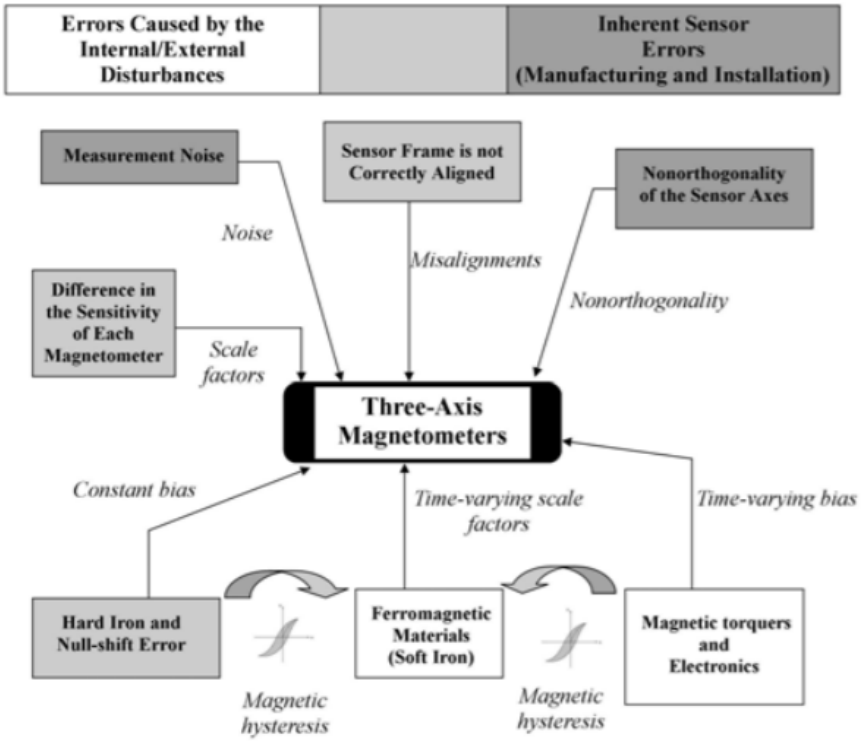

Figure 2.16: Summary of magnetic sensor errors

2.4 Attitude Representation

There are numerous different alternatives for representing the attitude of a system via vectors of three parameters, four parameters, and different sized matrices [49]. A brief survey about some of these alternatives can be given as following.

2.4.1 Euler Angles

Introduced by Leonhard Euler for representing the orientation of a system w.r.t. the fixed reference frame with three successive rotations, the theorem by his own words states that "Any two independent orthonormal coordinate frames can be related by a sequence of rotations (not more than three) about coordinate axes, where no two successive rotations may be about the same axis." [50]. Whereas intuitively easy to understand, choice uncertainty between different sequences (at least twelve) and singularity/ambiguity problems make this methodology disadvantageous for applications [51]. Figure 2.6 demonstrates conventional ZYX Euler angle rotation sequence as following [52].

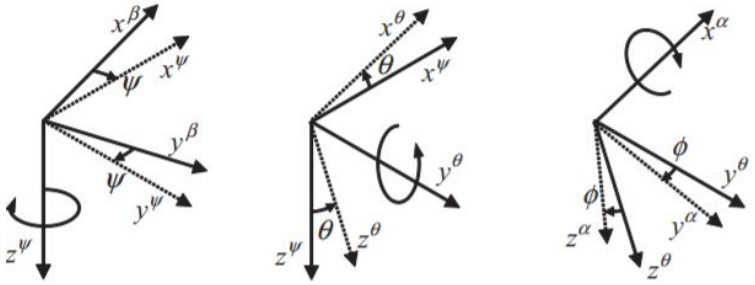

Figure 2.17: ZYX Euler angle rotation sequence

2.4.2 Euler-Rodrigues Symmetric Parameters and Quaternions

2.4.2.1 Rodrigues' Rotation Formula

In order to compute the rotation matrix $\mathbf{R}$ in the 3D rotation group, SO(3), corresponding to a rotation by an angle θ about a fixed reference axis specified by the unit vector $\mathbf{r} = (r_x, r_y, r_z)\varepsilon\mathbb{R}^3$, Olinde Rodrigues proposed following solution scheme intuitively straightforward to understand geometrically [53, 54].

$$\mathbf{R}(\mathbf{r}, \theta) = \mathbf{I_3} + \widetilde{\mathbf{r}} \sin\theta + (1 - \cos\theta)\widetilde{\mathbf{r}}^2. \tag{2.10}$$

The symbol (~) represents the cross-product operator which is transforming a column vector $\mathbf{c} = \begin{bmatrix} c_1 & c_2 & c_3 \end{bmatrix}^T$ to a matrix form as,

$$\widetilde{\boldsymbol{c}} = \begin{bmatrix} 0 & -c_3 & c_2 \\ c_3 & 0 & -c_1 \\ -c_2 & c_1 & 0 \end{bmatrix}. \tag{2.11}$$

2.4.2.2 Symmetric Parameters and Quaternions

Euler-Rodrigues parameters which are closely connected with the quaternions, were developed step by step by Euler and Rodrigues but unlike the methods they individually introduced, Euler-Rodrigues approach utilizes a different parameterization technique [49]. In order to compute the rotation matrix **R** in the 3D rotation group,SO(3), corresponding to a rotation by an angle θ about a fixed reference axis specified by the unit vector $\mathbf{r} = (r_x, r_y, r_z)\varepsilon\mathbb{R}^3$, Euler-Rodrigues proposed following symmetrical parameters.

$$\beta_0 = \cos(\frac{\theta}{2}), \tag{2.12}$$

$$\boldsymbol{\beta} = [\beta_1, \beta_2, \beta_3] = \sin(\frac{\theta}{2})\mathbf{r}, \tag{2.13}$$

These parameters are constrained by following expression,

$$\beta_0^2 + \boldsymbol{\beta}.\boldsymbol{\beta} = 1, \tag{2.14}$$

and this means that the symmetrical parameters can be also used for defining a unit quaternion proposed by W.R. Hamilton and the relation between Hamilton's quaternions and Euler-Rodrigues parameters are shown as following [55].

$$\mathbf{q} = q_0 + \mathbf{q}_1 + \mathbf{q}_2 + \mathbf{q}_3, \tag{2.15}$$

$$q_0 = \beta_0 = \cos(\frac{\theta}{2}), \tag{2.16}$$

$$\mathbf{q}_{vec} = [\mathbf{q}_1, \mathbf{q}_2, \mathbf{q}_3] = [\beta_1\mathbf{i}, \beta_2\mathbf{j}, \beta_3\mathbf{k}], \tag{2.17}$$

where **i**, **j** and **k** denote the basic quaternions, spatial axes on space. Therefore, resultant rotation matrix, **R**, can be shown as following [51].

$$\mathbf{R}(\mathbf{q}) = \begin{bmatrix} 2(q_0^2 + q_1^2) - 1 & 2(q_1 q_2 - q_0 q_3) & 2(q_1 q_3 + q_0 q_2) \\ 2(q_1 q_2 + q_0 q_3) & 2(q_0^2 + q_2^2) - 1 & 2(q_2 q_3 - q_0 q_1) \\ 2(q_1 q_3 - q_0 q_2) & 2(q_2 q_3 + q_0 q_1) & 2(q_0^2 + q_3^2) - 1 \end{bmatrix}. \tag{2.18}$$

2.4.3 Cayley-Klein Parameters

Four complex parameters, denoted by α-β-γ-δ, defined by Cayley and Klein are also used for characterizing the orientation of the system. In terms of these parameters, the rotation matrix can be extracted with following expression [56].

$$\mathbf{R}(\alpha,\beta,\gamma,\delta) = \begin{bmatrix} 0.5(\alpha^2 - \gamma^2 + \delta^2 - \beta^2) & 0.5\mathbf{i}(\gamma^2 - \alpha^2 + \delta^2 - \beta^2) & \gamma\delta - \alpha\beta \\ 0.5\mathbf{i}(\alpha^2 + \gamma^2 - \delta^2 - \beta^2) & 0.5(\alpha^2 + \gamma^2 + \delta^2 + \beta^2) & -\mathbf{i}(\alpha\beta + \gamma\delta) \\ \beta\delta - \alpha\gamma & \mathbf{i}(\alpha\gamma + \beta\delta) & \alpha\delta + \beta\gamma \end{bmatrix}. \tag{2.19}$$

2.4.4 Axis-Angle Representation

Represented with "axis", specified by unit vector $\mathbf{r} = (r_x, r_y, r_z)$ that is denoting the axis of rotation, and angle θ that is denoting the magnitude of rotation w.r.t. the axis of rotation, axis-angle representation is another straightforward methodology to interpret the attitude of a system. The one can obtain rotation matrix via applying Rodrigues' rotation formula in this representation and following result for rotation matrix is to be achieved.

$$\mathbf{R}(\mathbf{r},\theta) = \begin{bmatrix} (1-\cos\theta)r_x^2 + \cos\theta & (1-\cos\theta)r_x r_y - r_z\sin\theta & (1-\cos\theta)r_x r_z + r_y\sin\theta \\ (1-\cos\theta)r_x r_y + r_z\sin\theta & (1-\cos\theta)r_y^2 + \cos\theta & (1-\cos\theta)r_y r_z - r_x\sin\theta \\ (1-\cos\theta)r_x r_z - r_y\sin\theta & (1-\cos\theta)r_y r_z + r_x\sin\theta & (1-\cos\theta)r_z^2 + \cos\theta \end{bmatrix}. \tag{2.20}$$

2.4.5 Direction Cosine Matrix

Since Euler angles depiction has the singularity problem for large interval of rotations and quaternion representation, even though being widely used in 3-D orientation estimation, is inefficient in 2-D attitude estimation because there are two redundant parameters, in this study, DCM representation is chosen for attitude representation.

Moreover, only three parameters of the DCM is to be used for roll and pitch angle estimation even though this matrix has nine parameters within so that this makes DCM approach as the best candidate for the current problem as stated in [24]. Let I and S demonstrate the inertial and the sensor frame coordinates, respectively. ${}^{I}_{S}\mathbf{R}$ is the DCM of the sensor frame with respect to the inertial frame and to be denoted as $\mathbf{R}$ for convenience. Using the conventional Z-Y-X Euler angle sequence, $\mathbf{R}$ can be constructed as following,

$$\mathbf{R} = \begin{bmatrix} c\alpha c\beta & c\alpha s\beta s\gamma - s\alpha c\gamma & c\alpha s\beta c\gamma + s\alpha s\gamma \\ s\alpha c\beta & s\alpha s\beta s\gamma + c\alpha c\gamma & c\alpha s\beta s\gamma - c\alpha s\gamma \\ -s\beta & c\beta s\gamma & c\beta c\gamma \end{bmatrix}. \tag{2.21}$$

In this representation, α (yaw), β (pitch), and γ (roll) are the rotation angles about the Z, Y, and X axes, respectively and c and s stand for cosine and sine trigonometric functions. It is obvious that the two-axis attitude estimation is able to be executed using only the last row of matrix $\mathbf{R}$ whose entries are functions of roll and pitch angles, which are the angles to be estimated. These angles can be evaluated from basic trigonometric identities as,

$$\gamma = \tan^{-1}\left(\frac{R_{32}}{R_{33}}\right), \tag{2.22}$$

$$\beta = \tan^{-1}\left(\frac{-R_{31}}{\sqrt{R_{32}^2 + R_{33}^2}}\right). \tag{2.23}$$

Here $\mathbf{R}_{ij}$ represents $(i,j)^{th}$ entry of matrix $\mathbf{R}$. Therefore, this last row can also be used as the state vector for this work as following,

$$\mathbf{x} = \mathbf{R}^T\mathbf{e} = \begin{bmatrix} R_{31} \\ R_{32} \\ R_{33} \end{bmatrix}, \tag{2.24}$$

where $\mathbf{e}$ vector is defined as $\mathbf{e} = \begin{bmatrix} 0 & 0 & 1 \end{bmatrix}^T$. Note that when $\mathbf{R}_{31} = \pm 1$ singularity arises for this used Euler angle sequence. If the platform never experiences $\pm 90^\circ$ pitch angle such singularity will not occur. Otherwise, method of sequential rotations can be used to avoid singularity [57]. Hereafter, left superscript "S" will be omitted for convenience.

Table 2.2 demonstrates the advantages and disadvantages of representing the attitude using the common three methods mentioned previously.

Table 2.2: Summary of the various methods for the parameterization of the attitude

Representation Methods	Advantages	Disadvantages
Euler Angles	Three parameters	Non-linear equations Order of rotation is important Singularity problem
DCM	Linear differential equations No singularity	9 parameters Computational complexity
Quaternion	Four parameters No singularity Simple computation	Hard to understand intiuitively Transformation matrix is difficult to extract

2.5 Coordinate Transformations

Transformation between the coordinate frames can be accomplished via the methods mentioned on previous sub-sections, in other words, direction cosines, Euler angles or quaternions. Since all of these methods are able to provide direction cosine matrices, in this study, transformations are done with DCMs.

2.5.1 Transformation Between ECI and ECEF

As shown in Figure 2.1, the reason behind the required transformation between ECI and ECEF frames is the Earth's rotation rate denoted with $\boldsymbol{\omega}_e$ that is approximately 7.2921159×10^{-5} radians per second. ${}^{E}_{I}\mathbf{R}$ is the DCM which is responsible for executing transformation from the inertial frame to the ECEF frame [1].

$$ {}^{E}_{I}\mathbf{R} = \begin{bmatrix} \cos\omega_e t & \sin\omega_e t & 0 \\ -\sin\omega_e t & \cos\omega_e t & 0 \\ 0 & 0 & 1 \end{bmatrix}. \tag{2.25} $$

Inverse transformation, from ECEF to the inertial frame can be done via taking the inverse of ${}^{E}_{I}\mathbf{R}$ which is resulting with matrix ${}^{I}_{E}\mathbf{R}$ since rotation matrices are orthogonal.

$$ {}^{I}_{E}\mathbf{R} = ({}^{E}_{I}\mathbf{R})^{-1} = ({}^{E}_{I}\mathbf{R})^{T}. \tag{2.26} $$

2.5.2 Transformation Between Navigation Frame and ECEF

${}^{E}_{N}\mathbf{R}$ is the DCM which is responsible for executing transformation from the navigation frame to the ECEF frame and in order to do this transformation, the navigation frame must be rotated $\theta - 90$ degrees around its east axis and then $-90 - \lambda$ around its z-axis where θ and λ denote the latitude and the longitude [1].

$$ {}^{E}_{N}\mathbf{R} = \begin{bmatrix} -\sin\lambda & -\sin\theta\cos\lambda & cos\theta\cos\lambda \\ \cos\lambda & -\sin\theta\sin\lambda & cos\theta\sin\lambda \\ 0 & \cos\theta & \sin\theta \end{bmatrix}. \tag{2.27} $$

Inverse transformation, from ECEF to the navigation frame can be done via taking the inverse of ${}^{E}_{N}\mathbf{R}$ which is resulting with matrix ${}^{N}_{E}\mathbf{R}$ since rotation matrices are orthogonal.

$$ {}^{N}_{E}\mathbf{R} = ({}^{E}_{N}\mathbf{R})^{-1} = ({}^{E}_{N}\mathbf{R})^{T}. \tag{2.28} $$

2.5.3 Transformation Between Navigation Frame and Wander Frame

As mentioned while describing the wander frame, there is a wander angle, α, between the navigation and wander frames. The wander frame contains a rotation about z-axis of the navigation frame by this angle. So, ${}^{N}_{W}\mathbf{R}$ is the DCM which is responsible for executing transformation from the wander frame to the navigation frame [1].

$$ {}^{N}_{W}\mathbf{R} = \begin{bmatrix} \cos\alpha & -\sin\alpha & 0 \\ \sin\alpha & \cos\alpha & 0 \\ 0 & 0 & 1 \end{bmatrix}. \tag{2.29} $$

Inverse transformation, from navigation to the wander frame can be done via taking the inverse of ${}^{N}_{W}\mathbf{R}$ which is resulting with matrix ${}^{W}_{N}\mathbf{R}$ since rotation matrices are orthogonal.

$$ {}^{W}_{N}\mathbf{R} = ({}^{N}_{W}\mathbf{R})^{-1} = ({}^{N}_{W}\mathbf{R})^{T}. \tag{2.30} $$

CHAPTER 3

ATTITUDE ESTIMATION METHODS

3.1 Static Attitude Determination Methods

As mentioned in the introduction section, Grace Wahba, a retired statistician today, proposed a problem as known as "Wahba's Problem", which becomes the main question behind spacecraft attitude determination, in 1965 during her graduate years in Stanford and Maryland Universities [58]. The question is basically to find the appropriate, three dimensional orthogonal $\mathbf{R}$ matrix that is minimizing the following cost function.

$$J(\mathbf{R}) = \frac{1}{2}\sum_{i=1}^{N} a_i |\mathbf{b}_i - \mathbf{R}\mathbf{r}_i|^2, \tag{3.1}$$

where, a_i is the set of non-negative weighting factors, $\mathbf{r}_i$ and $\mathbf{b}_i$ denote the unit vector measurements resolved in the reference frame and body frame respectively for each observation. After this point, numerous solutions regarding to extract an optimal solution for the problem are proposed and detailed studies can be found in literature. Following, some of the most recognized methods for attitude determination via deterministic methods are listed [59].

3.1.1 TRIAD Method

While the space race was escalated between the super-powers of the world, numerous technological improvements, thought to be impossible to achieve, became reality step-by-step. Satellite navigation was one of the important disciplines during these years, and scientists were seeking for a solution that can be used in space environment for accurately navigating the satellites.

Johns Hopkins Applied Physics Laboratories was one of the centers for these studies, and Harold Black was one of the people who were responsible United States' transit satellite system. At this time, in 1964, TRIAD methodology was developed by Black and this approach becomes one of the earliest solutions for spacecraft orientation determination before the researchers started to be interested with Wahba's problem. Black's classical solution follows the steps to be given as following. Two unit vector measurements resolved in body frame ($\mathbf{b}_1$, $\mathbf{b}_2$) form the first triad ($\mathbf{M}_b$), while their navigation frame counterparts ($\mathbf{r}_1$, $\mathbf{r}_2$) form the second triad ($\mathbf{M}_r$). It is important to emphasize that TRIAD algorithm assumes one of the unit vector measurements is less accurate than other one and this less accurate information is to be disregarded [60].

$$\mathbf{M}_b = \begin{bmatrix} \mathbf{b}_1 & \frac{\mathbf{b}_1 \times \mathbf{b}_2}{|\mathbf{b}_1 \times \mathbf{b}_2|} & \mathbf{b}_1 \times \frac{\mathbf{b}_1 \times \mathbf{b}_2}{|\mathbf{b}_1 \times \mathbf{b}_2|} \end{bmatrix}, \tag{3.2}$$

$$\mathbf{M}_r = \begin{bmatrix} \mathbf{r}_1 & \frac{\mathbf{r}_1 \times \mathbf{r}_2}{|\mathbf{r}_1 \times \mathbf{r}_2|} & \mathbf{r}_1 \times \frac{\mathbf{r}_1 \times \mathbf{r}_2}{|\mathbf{r}_1 \times \mathbf{r}_2|} \end{bmatrix}. \tag{3.3}$$

Therefore, the orthogonal direction cosine responsible for transformation between navigation and body frames can be obtained as following via TRIAD.

$$\mathbf{M}_r = \mathbf{R}\mathbf{M}_b, \tag{3.4}$$

$$\mathbf{R} = \mathbf{M}_r \mathbf{M}_b^{-1} = \mathbf{M}_r \mathbf{M}_b^T. \tag{3.5}$$

In addition, TRIAD algorithm itself facilitates to refine measurements coming from sensors before Kalman or complementary filtering operations and today it is still a preferable algorithm for various attitude determination tasks [39]. The ways to improve TRIAD method are basically using more measurements and scaling the measurements according to their weights. Following methods are devoted for improving the TRIAD, one of the earliest solutions for attitude determination problem.

3.1.2 Davenport's q-Method

In 1968, Paul Davenport, a NASA mathematician published his studies about finding a solution for Wahba's problem. The solution he came up with is known Davenport's q-Method today, and is the first elegant and useful algorithm for attitude determination applications [61].

In his famous solution that was used in NASA's HEAO-1 and HEAO-B attitude determination system algorithms, Davenport defined the loss function in appropriate way via using the orthogonality of attitude matrix $\mathbf{R}$ and rewriting (3.1) as following [62].

$$|\mathbf{b}_i - \mathbf{R}\mathbf{r}_i|^2 = |\mathbf{b}_i|^2 + |\mathbf{R}\mathbf{r}_i|^2 - 2\mathbf{b}_i \cdot (\mathbf{R}\mathbf{r}_i) = 2 - 2tr(\mathbf{R}\mathbf{r}_i\mathbf{b}_i^T), \tag{3.6}$$

and the loss/cost function becomes,

$$J(\mathbf{R}) = \lambda_0 - tr(\mathbf{R}\mathbf{B}^T), \tag{3.7}$$

where,

$$\lambda_0 = \sum_{i=1}^{N} a_i, \tag{3.8}$$

$$\mathbf{B} = \sum_{i=1}^{N} a_i \mathbf{b}_i \mathbf{r}_i^T. \tag{3.9}$$

Davenport then realized that the loss function is minimized when $J^{'}(\mathbf{R})$ is to be maximized. The expression for the derivative of loss function can be given as following.

$$J^{'}(\mathbf{R}) = \sum_{i=1}^{N} \mathbf{r}_i \mathbf{R} \mathbf{b}_i. \tag{3.10}$$

Before to proceed, it is important to state that Davenport preferred to parameterize the attitude direction cosine matrix in terms of quaternions and then gave the derivative of loss function. Quaternion parameterization of DCM is executed in line with quaternion conventions defined in (2.11).

$$\mathbf{R(q)} = (q_0^2 - \mathbf{q} \cdot \mathbf{q})\mathbf{I}_3 + 2\mathbf{q}\mathbf{q}^T - 2q_0\widetilde{\mathbf{q}}. \tag{3.11}$$

Note that, $\mathbf{q}$ is defined in line with (2.15). Now it is possible to substitute (3.11) into (3.10), and after tedious and considerable matrix operations, following result obtained.

$$J^{'}(\mathbf{R(q)}) = \mathbf{q}^T \mathbf{K} \mathbf{q}, \tag{3.12}$$

where,

$$\mathbf{K} = \begin{bmatrix} \sigma & \mathbf{z}^T \\ \mathbf{z} & \mathbf{S} - \sigma\mathbf{I}_3 \end{bmatrix}, \tag{3.13}$$

$$\sigma = tr(\mathbf{B}), \tag{3.14}$$

$$\mathbf{S} = \mathbf{B} + \mathbf{B}^T, \tag{3.15}$$

$$\mathbf{z} = \begin{bmatrix} B_{23} - B_{32} \\ B_{31} - B_{13} \\ B_{12} - B_{21} \end{bmatrix}. \tag{3.16}$$

Thus, the optimal attitude quaternion ($\mathbf{q}_{opt}$) is an eigenvector of matrix $\mathbf{K}$.

$$\mathbf{K}\mathbf{q}_{opt} = \lambda_{max}\mathbf{q}_{opt}, \tag{3.17}$$

This choice of matrix $\mathbf{K}$ as the largest eigenvector ensures to maximize $J'(\mathbf{R})$ while minimizing the main cost function. After this point, the problem turns into the eigen-problem, the hardest part for the commerical computers in old days, that can be solved in different ways.

3.1.3 Quaternion Estimator Method

Launched in 1979, NASA's MAGSAT mission satellite carried a novel algorithm with itself developed by Malcolm D. Shuster and known as QUEST algorithm that aims to solve Wahba's problem via a different perspective and within an efficient computational time interval [63]. The QUEST algorithm aims to provide attitude estimation results within acceptable frequency interval which q-Method is not able to do. Now, if one thinks (3.17) as eigenvalue problem, following expression is to be obtained.

$$(\lambda_{max}\mathbf{I}_4 - \mathbf{K})\mathbf{q}_{opt} = \mathbf{0}_4, \tag{3.18}$$

and this expression can be split into two equations as,

$$(\lambda_{max} - \sigma)q_0 - \mathbf{z}^T\mathbf{q} = 0, \tag{3.19}$$

$$((\lambda_{max} + \sigma)\mathbf{I}_3 - \mathbf{S})\mathbf{q} - q_0\mathbf{z} = 0. \tag{3.20}$$

If the characteristic function of (3.13) is given, one can obtain a fourth degree quartic equation as following.

$$((\lambda_{max}tr(\mathbf{B}))\mathbf{det}[(\lambda_{max} + \sigma)\mathbf{I}_3 - \mathbf{S})] - \mathbf{z}^T\mathbf{adj}[(\lambda_{max} + \sigma)\mathbf{I}_3 - \mathbf{S})]\mathbf{z} = 0. \tag{3.21}$$

After this point, with adequate matrix algebra, one is able to obtain the largest root of the quartic function via using Newton-Raphson iteration. Main advantage of the QUEST algorithm is its computational efficiency and robustness.

3.1.4 Singular Value Decomposition Technique

Rather than to deal with quaternions like in Davenport's and Shuster's methods, Markley proposed a matrix-based solution scheme for Wahba's problem using the SVD which is dealing with direction cosine matrices. Reported by Markley, even though Davenport's and Shuster's methodologies behave more efficient and faster than his own algorithm, the SVD is still preferable algorithm since it is able to provide eigenvalues and eigenvectors of covariance matrices that facilitate the analysis process [61]. SVD of the matrix **B** can be given as,

$$\mathbf{B} = \mathbf{U}\mathbf{\Sigma}\mathbf{V}^T = \mathbf{U}diag([s_1 \quad s_2 \quad s_3])\mathbf{V}^T, \tag{3.22}$$

where $s_1 \geq s_2 \geq s_3 \geq 0$, and matrices **U** and **V** are orthagonal. Thus, after considerable matrix algebra, the optimal DCM, attitude matrix of the system can be given as following [64].

$$\mathbf{R}_{opt} = \mathbf{U}diag([1 \quad 1 \quad det\mathbf{U} \quad det\mathbf{V}])\mathbf{V}^T. \tag{3.23}$$

3.1.5 Estimator of Optimal Quaternion Method

Daniel Mortari's ESOQ method avoids the requirement for explicit rotations via dealing with the components of the quaternion more symmetrically than QUEST methodology. Even though the strategy behind to locate the maximum magnitude component of the quaternion and to determine λ_{max} via Newton-Raphson iteration of the **K** matrix of Davenport, Mortari observed that the optimal quaternion is to be evaulated by normalizing not only the fourth column but any column of $adj(\lambda_{max}\mathbf{I}_4 - \mathbf{K})$. Whereas ESOQ might be preferred in order to exchange some computational burden with straightforward indexing operations, it should not be forgotten that QUEST method has a long history along the wide range of successful applications [65].

3.1.6 Fast Optimal Attitude Matrix Method

FOAM method carries some of the same features with SVD methodology as QUEST carries the similar features of Davenport's method. Computation of λ_{max} is done iteratively and simple matrix operations facilitates the determination of optimal attitude matrix via avoiding singular value decomposition [66].

3.2 Complementary Filtering

The main principle behind the complementary filtering for attitude estimation can be explained with following words. The attitude estimation can be executed accurately if the motion of a body remains smooth and constant since the measurements from accelerometer and magnetometer are relatively accurate and reliable at this time while the calculated attitude from gyroscope integration is to diverge within a very short period because of the gyroscope's characteristic errors. On the other hand, if the motion of a body becomes agile, the accelerometer's output is disturbed by external acceleration that makes the estimated attitude unreliable while the gyroscope can mitigate such errors at this time. So, it can be stated that accelerometer and gyroscope can "complement" each other in the frequency domain and this frequency-based behaviour of the two inertial sensors is the fundamental principle of attitude estimation from inertial sensors using complementary filters [67]. So, in this study, as benchmark methods, two of the most common CFs are selected. These are Mahony's and Madgwick's filters, used in wide perspective for orientation estimation.

3.2.1 Mahony's Filter

Mahony presents a complementary filtering method which is basically a proportional-integral compensation approach to the attitude estimation problem via fusing the gyroscope and accelerometer measurements [25]. After obtaining gyro and accelerometer measurements, firstly, orientation error is calculated by using accelerometer measurements while gyro measurements are updated with PI compensation of acceleration effect.

Then, orientation incremental calculation and finally, numerical integration for obtaining the estimated quaternion can be done. Figure 3.1. demonstrates the visual overview of Mahony's filter [68].

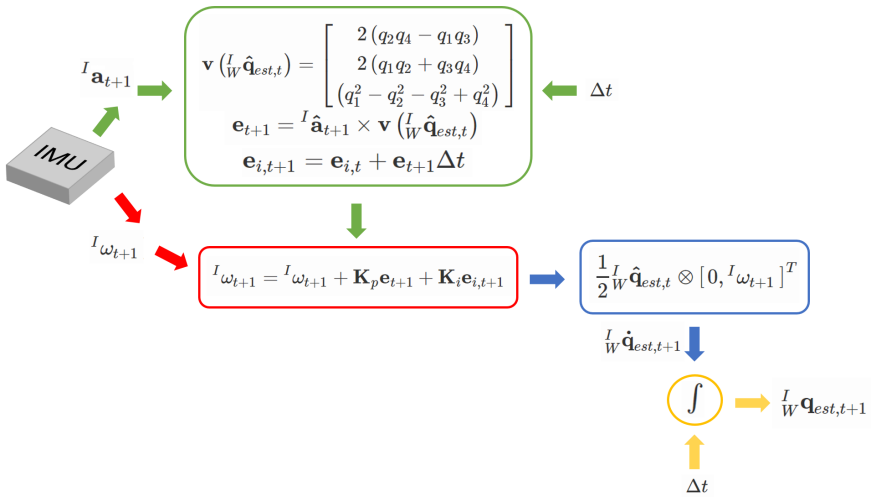

Figure 3.1: Overall algorithm scheme of Mahony's filter

Steps of Mahony's algorithm can be summarized via interpreting Figure 3.1. as following,

- **Step 1:** Acquisition of Sensor Measurements,
- **Step 2:** Orientation Error Computation via using Accelerometer Measurements,

$$\mathbf{v}({}^{I}_{W}\mathbf{q}_{est,t}) = \begin{bmatrix} 2(q_2q_4 - q_1q_3) \\ 2(q_1q_2 + q_3q_4) \\ (q_1^2 - q_2^2 - q_3^2 + q_4^2) \end{bmatrix}, \tag{3.24}$$

$$\mathbf{e}_{t+1} = {}^{I}\mathbf{a}_{t+1} \times \mathbf{v}({}^{I}_{W}\mathbf{q}_{est,t}), \tag{3.25}$$

$$\mathbf{e}_{i,t+1} = \mathbf{e}_{i,t+1} + \mathbf{e}_{t+1}\Delta t. \tag{3.26}$$

- **Step 3:** Updating the Gyroscope Measurements with PI Compensation,

$${}^{I}\omega_{t+1} = {}^{I}\omega_{t+1} + \mathbf{K}_p\mathbf{e}_{t+1} + \mathbf{K}_i\mathbf{e}_{i,t+1}. \tag{3.27}$$

- **Step 4:** Quaternion Derivative Calculation via using Gyroscope Measurements,

$$ {}^{I}_{W}\dot{q}_{\omega,t+1} = 0.5 {}^{I}_{W}\mathbf{q}_{est,t} \otimes [0 {}^{I}\omega_{t+1}]^{T}. \tag{3.28} $$

- **Step 5:** Computation of the Estimated Quaternion via Numerical Integration.

$$ {}^{I}_{W}\mathbf{q}_{est,t+1} = {}^{I}_{W}\mathbf{q}_{est,t} + {}^{I}_{W}\dot{q}_{\omega,t+1}\Delta t. \tag{3.29} $$

It is important to emphasize that these steps should be repeated in each sampling and only tunable parameters of the algorithm are PI gains K_p and K_i.

3.2.2 Madgwick's Filter

Madgwick treats the attitude estimation as a minimization problem and proposes a CF method, which is basically depending on the gradient decent strategy that uses the steepest decent algorithm to solve the problem recursively [26]. After obtaining gyro and accelerometer measurements, firstly, orientation incremental components from accelerometer and gyro are independently calculated. It is important to emphasize that the orientation increment from accelerometer is compensated with steepest decent gradient algorithm against disturbances and this algorithm is basically controlled by one parameter. Then, orientation incremental calculation and finally, numerical integration for obtaining the estimated quaternion can be done. Figure 3.2. demonstrates the visual overview of Madgwick's filter [69].

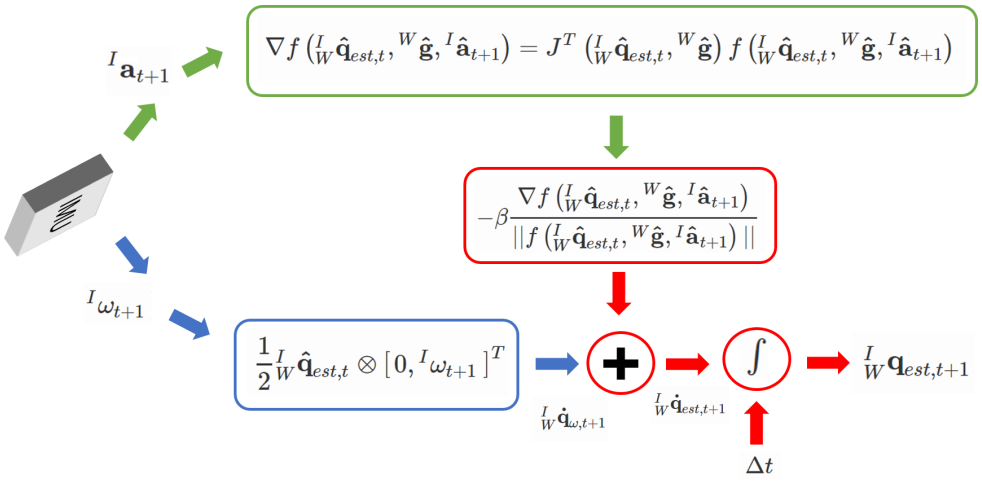

Figure 3.2: Overall algorithm scheme of Madgwick's filter

Steps of Madgwick's algorithm can be summarized via interpreting Figure 3.2. as following,

- **Step 1:** Acquisition of Sensor Measurements,
- **Step 2:** Quaternion Derivative Calculation via using Accelerometer Measurements,

$$\nabla \mathbf{f}({}^{I}_{W}\mathbf{q}_{est,t}, {}^{W}\mathbf{g}, {}^{I}\mathbf{a}_{t+1}) = J^{T}({}^{I}_{W}\mathbf{q}_{est,t}, {}^{W}\mathbf{g})\mathbf{f}({}^{I}_{W}\mathbf{q}_{est,t}, {}^{W}\mathbf{g}, {}^{I}\mathbf{a}_{t+1}). \tag{3.30}$$

- **Step 3:** Quaternion Derivative Calculation via using Gyroscope Measurements,

$${}^{I}_{W}\dot{q}_{\omega,t+1} = 0.5 {}^{I}_{W}\mathbf{q}_{est,t} \otimes [0 {}^{I}\omega_{t+1}]^{T}. \tag{3.31}$$

- **Step 4:** Fusing the Information Sources (Accelerometer and Gyroscope).

$${}^{I}_{W}\dot{q}_{est,t+1} = 0.5 {}^{I}_{W}\mathbf{q}_{est,t} \otimes [0 {}^{I}\omega_{t+1}]^{T}. \tag{3.32}$$

$${}^{I}_{W}\mathbf{q}_{est,t+1} = {}^{I}_{W}\mathbf{q}_{est,t} + {}^{I}_{W}\dot{q}_{\omega,t+1}\Delta t. \tag{3.33}$$

It is important to emphasize that these steps should be repeated in each sampling and only tunable parameter of the algorithm is β which is the trade-off weighting parameter between the gyroscope and accelerometer measurements.

3.3 Kalman Filtering

In order to estimate the states of a linear dynamic systems containing white Gaussian noise with using the information from measurements of the system also corrupted with white Gaussian noise, the Kalman filter algorithm is widely used today in numerous disciplines [70]. Table 3.1 and Figure 3.3 demonstrate the terminology behind the Kalman filtering operation and overall summary of recursive Kalman filtering procedure respectively as following.

Table 3.1: Terminology of Kalman filtering

$\mathbf{\Phi}$: State transition matrix	**H**: Observation matrix
x: State vector	$\mathbf{P}_k(-)$: A priori estimation covariance matrix
$\hat{\mathbf{x}}_k(-)$: A priori value of the estimated state vector	$\mathbf{P}_k(+)$: A posteriori estimation covariance matrix
$\hat{\mathbf{x}}_k(+)$: A posteriori value of the estimated state vector	**w**: Process noise
z: Measurement vector	**v**: Measurement noise
K: Kalman gain	**Q**&**R**: Process and measurement noise covariance matrices

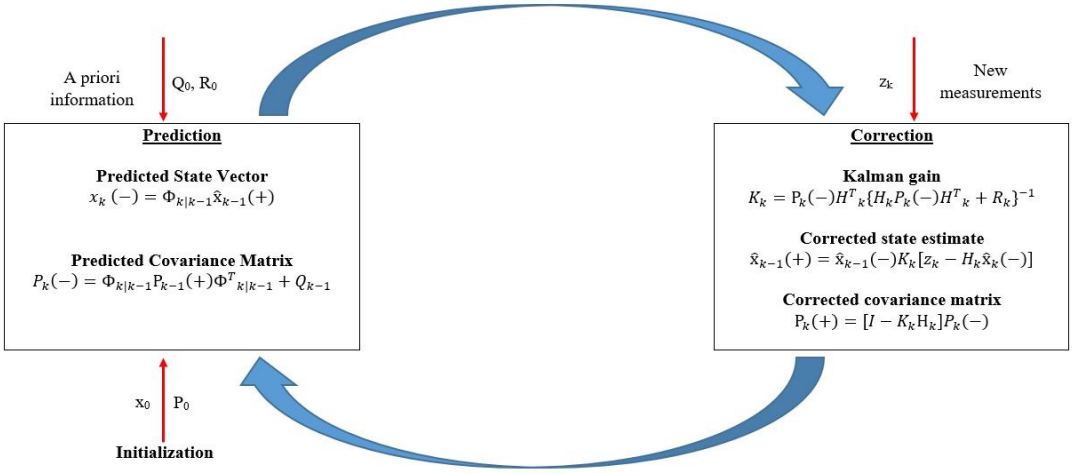

Figure 3.3: Overall summary of Kalman filtering procedure

Recursive characteristics of KF have been investigated on Figure 3.3, but more accurate algorithm flow diagram with following steps are provided for ease of understanding [1].

- **Step 1:** Initialization of the filter via providing initial estimates for states and estimation covariance matrix which is the measure of how much are known from the initial state estimates. Moreover, the measurement noise covariance matrix **R** and the system noise covariance matrix **Q** are required to be provided in order to initialize the filter. Prior knowledge about the system or adaptive structures within the algorithm are required to obtain the best estimates about the states.

- **Step 2:** Initial state is propagated via the aid of state transition matrix $\mathbf{\Phi}$, evaluated before the epoch, and propagated state is to be shown with $\hat{\mathbf{x}}_k(-)$ or $\mathbf{x}_k^-$.

This is the first prediction step within the algorithm.

- **Step 3:** In second step of prediction procedure in KF algorithm, estimation covariance matrix is propagated from previous epoch. State transition matrix, system noise covariance matrix and previous value of estimation covariance are responsible for the propagation and it is important to emphasize that if the system uncertainties/process noise is high, estimation covariance is to increase resulting with a lower confidence in the predicted states.

- **Step 4:** In the fourth step, correction/update procedure of the filter is executed. In this manner, Kalman gain $\mathbf{K}_k$ is computed and note that this calculation is dependent on a priori estimation covariance $\mathbf{P}_k(-)$, the measurement noise covariance matrix $\mathbf{R}_k$ and output design matrix $\mathbf{H}_k$.

- **Step 5:** In the second part of the correction/update procedure of the filter, predicted or a priori states $\hat{\mathbf{x}}_k(-)$ are corrected whenever a measurement is availabe for the algorithm. Corrected states are evaulated based on the difference between the actual measurements $\mathbf{z}_k$ and the predicted measurements $\mathbf{H}_k\hat{\mathbf{x}}_k(-)$. The new information about the states from correction come from this difference and when Kalman gain is relatively smaller, the new information obtained from the measurement is given less weight and the a priori estimate is considered to be relatively accurate but when Kalman gain is relatively bigger, difference is weighted heavier and it is added to the a priori estimate in order to update this to the a posteriori estimate $\hat{\mathbf{x}}_k(+)$.

- **Step 6:** Correction of the state estimate brings the end for one epoch of the recursive KF loop. After this, update of a priori estimation covariance is also done and it is propagated through to the a posteriori estimation covariance $\mathbf{P}_k(-)$ and KF goes a step further.

This brief discussion gives essentials about the Kalman filtering, but as mentioned in the literature survey, there are numerous different KF algorithms typically for nonlinear systems e.g. extended Kalman filter, unscented Kalman filter and serving different purposes.

3.3.1 Tilt Angles Estimation via Kalman Filtering

In this study, in order to execute Kalman filtering algorithm for attitude estimation, a linear KF structure is selected with following process and measurement models. The process model is governed by the following equation as,

$$\mathbf{x}_t^- = \mathbf{\Phi}_{t-1}\mathbf{x}_{t-1} + \mathbf{w}_{t-1}, \tag{3.34}$$

where "$-$" superscript denotes the prediction. $\mathbf{\Phi}$ is the state transition matrix that propagates the system states from previous time and $\mathbf{w}$ is the noise vector for the process model, assumed to be zero mean white Gaussian. In order to derive expressions for the state transition matrix and the process noise covariance matrix, time propagation of the rotation matrix, $\mathbf{R}$, is to be investigated. First order approximation for this propagation with gyro measurements can be given as,

$$\mathbf{R}_t = \mathbf{R}_{t-1}\left(\mathbf{I_3} + \Delta t\widetilde{\boldsymbol{\omega}}_{t-1}\right), \tag{3.35}$$

where Δt is the sampling time and $\widetilde{\boldsymbol{\omega}}_{t-1}$, is skew-symmetric matrix that includes ideal gyro rates of the body at time $t-1$. Instead of propagating the whole rotation matrix, the state vector itself can be propagated for estimating the attitude. The propagation of the state vector, given on the second section as the last row of DCM, can be given as following,

$$\mathbf{x}_t^- = \left(\mathbf{I_3} + \Delta t\widetilde{\boldsymbol{\omega}}_{t-1}\right)^T \mathbf{x}_{t-1}. \tag{3.36}$$

However, it is obvious that the ideal angular rates cannot be obtained by gyroscopes due to the existence of the measurement noise. Hence, (3.36) can be rewritten with the real gyroscope signal ($\mathbf{y}_G = {}^S\boldsymbol{\omega} + \mathbf{n}_G$) as following,

$$\mathbf{x}_t^- = \left(\mathbf{I_3} - \Delta t\widetilde{\mathbf{y}}_{G,t-1}\right)\mathbf{x}_{t-1} + \Delta t(-\widetilde{\mathbf{x}}_{t-1})\mathbf{n}_G. \tag{3.37}$$

Therefore, the state transition matrix and process noise can be defined from (3.37) as,

$$\mathbf{\Phi}_{t-1} = \mathbf{I_3} - \Delta t\widetilde{\mathbf{y}}_{G,t-1}, \tag{3.38}$$

$$\mathbf{w}_{t-1} = \Delta t(-\widetilde{\mathbf{x}}_{t-1})\mathbf{n}_G. \tag{3.39}$$

Finally, the process noise covariance matrix is obtained via expectation operator applied into the process noise. Thus, the resultant matrix ($\mathbf{Q}_{t-1}$) can be redefined as,

$$\mathbf{Q}_{t-1} = E[\mathbf{w}_{t-1}\mathbf{w}^T{}_{t-1}] = -\Delta t^2 \widetilde{\mathbf{x}}_{t-1}\mathbf{\Sigma}_G\widetilde{\mathbf{x}}_{t-1}, \tag{3.40}$$

where $\mathbf{\Sigma}_G$ is the noise covariance matrix of the gyroscope which is given as $\sigma_G^2\mathbf{I}_3$ assuming that the variance of gyro noise, σ_G^2, is distributed equal to all axes for the same gyro. On the other hand, the measurement model is governed by the following equation as,

$$\mathbf{z}_t = \mathbf{H}\mathbf{x}_t + \mathbf{v}_t, \tag{3.41}$$

where $\mathbf{z}$ is the measurement vector, $\mathbf{H}$ is the output matrix, relating the system states to the outputs and $\mathbf{v}$ is the noise vector for the measurement model, assumed to be zero mean white Gaussian.

$$\mathbf{H} = g\mathbf{I_3}, \tag{3.42}$$

$$\mathbf{v}_t = \boldsymbol{\varepsilon}_t + \mathbf{n}_A, \tag{3.43}$$

where $\boldsymbol{\varepsilon}_t$ and $\mathbf{n}_A$ are time-varying error during the motion and the accelerometer noise assumed to be uncorrelated, zero-mean white Gaussian noise. These two uncorrelated noise terms lead to a measurement noise covariance matrix as follows,

$$\mathbf{M}_t = E[\mathbf{v}_t\mathbf{v}_t^T] = \mathbf{\Sigma}_{acc} + \mathbf{\Sigma}_A. \tag{3.44}$$

Here $\mathbf{\Sigma}_A$ is the covariance matrix for the accelerometer measurement noise and $\mathbf{\Sigma}_{acc}$ is the covariance matrix for the acceleration modelling error. $\mathbf{\Sigma}_A$ is straightforward to set as $\sigma_A^2\mathbf{I}_3$ assuming that that the variance of accelerometer noise, σ_A^2, is distributed equal for all axes for the same accelerometer. However, time varying component of (3.44), $\mathbf{\Sigma}_{acc}$, cannot be analytically obtained since the actual external acceleration when the measurements are sampled at each step is unknown.

Following benchmark methods from the literature seek an efficient strategy for compensating the external disturbances via manipulating the measurement noise covariance matrix or adding magnetometer measurements into the system for estimating the attitude better.

3.3.1.1 Lee's Filter

Lee proposed a KF structure, which is able to adapt itself by automatically tuning the unknown component of the measurement noise covariance matrix [34]. As following formulation suggests this method assumes that the external acceleration is distributed the same along all axes:

$$\mathbf{\Sigma}_{acc} = 3^{-1} c_a^2 ||\mathbf{a}_{t-1}||^2 \mathbf{I_3}. \tag{3.45}$$

In order to derive expressions for the measurement model components, Lee split (2.3) into two equations given as,

$$\mathbf{a}_t^- = c_a \mathbf{a}_{t-1}, \tag{3.46}$$

$$\boldsymbol{\varepsilon}_t = \mathbf{a}_t - \mathbf{a}_t^-, \tag{3.47}$$

where $\mathbf{a}_t^-$ is the predicted (a priori) acceleration at time t, and $\mathbf{a}_{t-1}$ is the estimated (a posteriori) external acceleration at time $t-1$. Now, it is possible to rewrite (2.2) via inserting (2.3) into the acceleration term in (2.2) and showing the gravity vector resolved in the body frame as the product between the state vector and scalar gravity as following,

$$\mathbf{y}_{\mathbf{A},t} - c_a \mathbf{a}_{t-1} = g\mathbf{x}_t + \boldsymbol{\varepsilon}_t + \mathbf{n}_A. \tag{3.48}$$

Here, the scalar gravitational acceleration is given as $g = 9.81 m/s^2$. Therefore, via comparing (3.41) and the resultant equation, (3.48), $\mathbf{z}_t$ becomes,

$$\mathbf{z}_t = \mathbf{y}_{\mathbf{A},t} - c_a \mathbf{a}_{t-1}, \tag{3.49}$$

3.3.1.2 Harada's Filter

Harada proposed a switch-gain KF structure, which is able to adapt the measurement noise covariance matrix by switching its value based on external acceleration. During the highly disturbed/accelerated scenarios, the filter basically ignores the measurements coming from the accelerometer [71]. Following formulation demonstrates the logic of the algorithm where δ is the threshold and $\mathbf{z}_t = \mathbf{y}_{\mathbf{A},t}$.

$$\mathbf{\Sigma}_{acc} = \begin{cases} 0, & \text{if } |||\mathbf{y}_{\mathbf{A},t}|| - g| \leq \delta, \\ \infty, & \text{otherwise.} \end{cases} \tag{3.50}$$

3.3.2 Full Attitude/Orientation Estimation via Kalman Filtering

Rather than to evaluate the tilt angles (i.e. roll and pitch), some applications require the calculation of full attitude, orientation of the system. In this case, layout of MARG sensors is required and quaternion representation is preferred within the developed algorithms.

3.3.2.1 Guo's Filter

Guo et al proposed a quaternion-based fast Kalman filter algorithm in order to deal with the orientation estimation problem. In this method, the process model is formed via using kinematic quaternion equation while the attitude quaternion from accelerometer-magnetometer fusion is preferred as the backbone of the measurement model [72]. So, following equations demonstrate the prediction step of the algorithm using quaternion kinematic equation.

$$\mathbf{q}_t^- = \mathbf{I}_4 + \frac{\Delta t}{2}[\mathbf{\Omega}\times]\mathbf{q}_{t-1}, \tag{3.51}$$

$$\mathbf{P}_t^- = [\mathbf{I}_4 + \frac{\Delta t}{2}[\mathbf{\Omega}\times]]\mathbf{P}_{t-1}[\mathbf{I}_4 + \frac{\Delta t}{2}[\mathbf{\Omega}\times]]^T + \mathbf{Q}, \tag{3.52}$$

where,

$$[\mathbf{\Omega}\times] = \begin{bmatrix} 0 & -\omega_x & -\omega_y & -\omega_z \\ \omega_x & 0 & \omega_z & -\omega_y \\ \omega_y & -\omega_z & 0 & \omega_x \\ \omega_z & \omega_y & -\omega_x & 0 \end{bmatrix}. \tag{3.53}$$

After the prediction step, state and covariance correction can be done via the aid of Kalman gain as following.

$$\mathbf{K}_t = \mathbf{P}_t^-[\mathbf{P}_t^- + \mathbf{R}]^{-1}, \tag{3.54}$$

$$\mathbf{q}_t = \mathbf{q}_t^- + \mathbf{K}_t(\mathbf{q}_{meas,t} - \mathbf{q}_t^-), \tag{3.55}$$

$$\mathbf{P}_t = [\mathbf{I}_4 - \mathbf{K}_t]\mathbf{P}_t^-. \tag{3.56}$$

3.3.2.2 Dai's Filter

Dai et al proposed a lightweight quaternion-based extended Kalman filter algorithm in order to deal with the orientation estimation problem with low-cost sensor frameworks. In this method, the process model is formed via using kinematic quaternion equation similar to Guo's filter while a simplified measurement model formed by accelerometer and magnetometer measurements is used [33]. Following equations demonstrate the prediction step of the algorithm using quaternion kinematic equation.

$$\mathbf{q}_t^- = \mathbf{I}_4 + \frac{\Delta t}{2}[\mathbf{\Omega}\times]\mathbf{q}_{t-1}, \tag{3.57}$$

$$\mathbf{F}_t = \mathbf{I}_4 + \frac{\Delta t}{2}[\mathbf{\Omega}\times], \tag{3.58}$$

$$\mathbf{P}_t^- = \mathbf{F}_t\mathbf{P}_{t-1}\mathbf{F}_t^T + \mathbf{Q}, \tag{3.59}$$

After the prediction step, state and covariance correction can be done via the aid of Kalman gain. It is important to note that again the measurement vector is not sole attitude quaternion as Guo's study and one might expect that the computational time advantage is on Guo's filter. However, Dai stated that the LEKF is slightly faster than Guo's FKF and the reason is given as rather than to deal with extracting the attitude quaternion from accelerometer-magnetometer fusion, simplified measurement components are to reduce the computational time of the algorithm [33].

$$\mathbf{K}_t = \mathbf{P}_t^-\mathbf{H}_t[\mathbf{H}_t\mathbf{P}_t^-\mathbf{H}_t^T + \mathbf{R}]^{-1}, \tag{3.60}$$

$$\mathbf{z}_{meas,t} = \begin{bmatrix} a_x & a_y & a_z & \frac{a_y m_z - a_z m_y}{m_N} \end{bmatrix}^T \tag{3.61}$$

$$\mathbf{q}_t = \mathbf{q}_t^- + \mathbf{K}_t(\mathbf{z}_{meas,t} - \mathbf{H}_t\mathbf{q}_t^-), \tag{3.62}$$

$$\mathbf{P}_t = [\mathbf{I}_4 - \mathbf{K}_t\mathbf{H}_t]\mathbf{P}_t^-. \tag{3.63}$$

CHAPTER 4

ROBUST KALMAN FILTERING FOR ATTITUDE ESTIMATION

4.1 Adaptive Kalman Filtering with Noise Covariance Scaling

Adaptive measurement noise covariance scaling methodology is basically to change KF gain via scaling the measurement noise covariance matrix autonomously during the estimation process. Therefore, it means that the filter can adapt itself to this new environment via comparing theoretical and real values of the innovation covariance [40, 41] when there exist external disturbances on the measurement system so that these effects can be compensated. Definition of innovation in KF structure is,

$$\mathbf{e}_t = \mathbf{z}_t - \mathbf{H}\mathbf{x}_t^- \tag{4.1}$$

where $\mathbf{x}_t^-$ is the predicted state vector and $\mathbf{e}_t$ is the innovation sequence. Kalman filter gain changes with varying innovation covariance if there exist mismatches between the process and measurement models, therefore the innovation covariance after filter adaptation can be defined as following with KF gain,

$$\hat{\mathbf{C}}_{e_t} = \mathbf{H}\mathbf{P}_t^-\mathbf{H}^T + \mathbf{S}_t\mathbf{M}_t \tag{4.2}$$

$$\mathbf{K}_t = \mathbf{P}_t^-\mathbf{H}^T(\mathbf{H}\mathbf{P}_t^-\mathbf{H}^T + \mathbf{S}_t\mathbf{M}_t)^{-1} \tag{4.3}$$

where $\mathbf{P}_t^-$ is the predicted covariance matrix during the KF process and $\mathbf{S}_t$ is the measurement noise covariance matrix scaling factor (SF). If the real value of KF error exceeds the theoretical error, which can be shown as,

$$tr(\mathbf{e}_t\mathbf{e}_t^T) \geq tr(\mathbf{H}\mathbf{P}_t^-\mathbf{H}^T + \mathbf{M}_t) \tag{4.4}$$

filtering process must be done adaptively. In (4.4), $tr(.)$ denotes the trace operation of the related matrix.

There are two possible options for scaling the measurement noise covariance matrix, single-scale factor and multiple-scale factor options, respectively. The idea to apply this strategy into the attitude estimation problem is covered in one of our recent works [42]. For both approaches the common frame of the algorithm is similar and presented in the Figure 4.1. Calculation of $\mathbf{\Sigma}_{acc}$ differs in two approaches as will be explained.

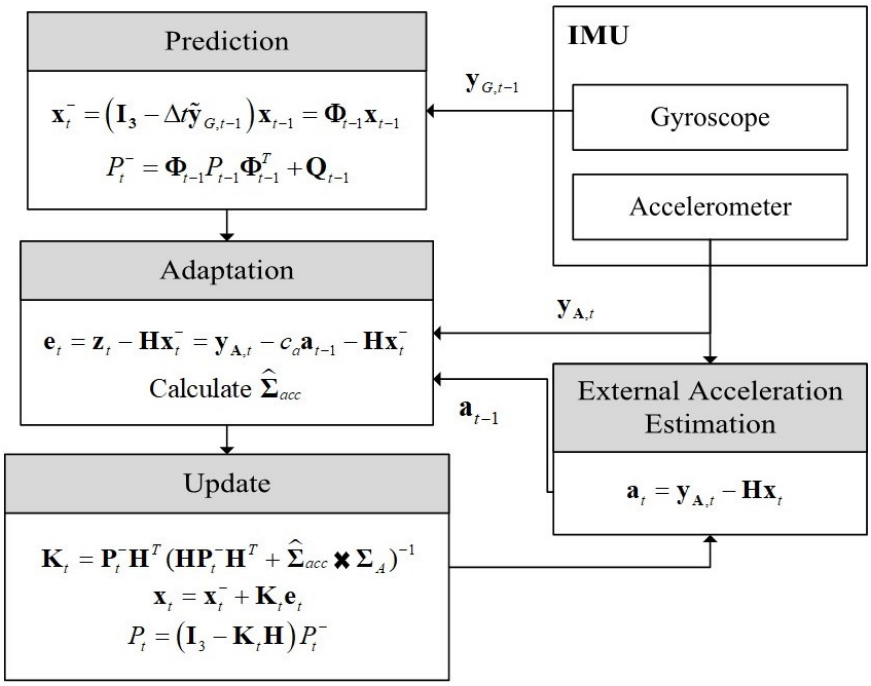

Figure 4.1: Common frame for the proposed RKF with scaling algorithms

4.1.1 Single-Scale Factor Method

In the first approach, in the SSF is introduced directly to modify the $\mathbf{M}_t$ matrix as in (4.3). In order to obtain the SSF, first, let us insert $\mathbf{S}_t$ into the inequality in (4.4) and take the condition where two innovations are equal as the basis as,

$$tr(\mathbf{e}_t \mathbf{e}_t^T) = tr(\mathbf{H}\mathbf{P}_t^- \mathbf{H}^T) + S_t tr(\mathbf{M}_t) \tag{4.5}$$

therefore, S_t can be expressed as,

$$S_t = \frac{\mathbf{e}_t^T \mathbf{e}_t - tr\left\{\mathbf{H}_t \mathbf{P}_t^- \mathbf{H}_t^T\right\}}{tr\left\{\mathbf{M}_t\right\}} \tag{4.6}$$

If there is no external acceleration or disturbance detected i.e. condition given in (4.4) is not met, $\mathbf{S}_t$ simply becomes $\mathbf{S}_t = 1$.

4.1.2 Multiple-Scale Factor Method

In the second approach, the MSF methodology is introduced. Rather than to adaptively tune the Kalman gain via scalar factor, it becomes appropriate to use a matrix structure with multiple factors since SSF approach rejects the measurements from all channels, even if the external acceleration is sensed in one direction. Therefore, using the same method for derivation of the SSF, but instead estimating a matrix composed of multiple factors $\mathbf{S}_t$ can be written as,

$$\mathbf{S}_t = (\mathbf{e}_t\mathbf{e}_t^T - \mathbf{H}\mathbf{P}_t^-\mathbf{H}^T)\mathbf{M}_t^{-1} \tag{4.7}$$

Same as mentioned, if there is no external acceleration or disturbance detected i.e. condition given in (4.4) is not ensured again, now, $\mathbf{S}_t$ simply becomes as following.

$$\mathbf{S}_t = diag(s_1, s_2, s_3), \tag{4.8}$$

$$s_i = max\left\{1, \mathbf{S}_{ii}\right\}, i = 1, 2, 3. \tag{4.9}$$

It is very important to note that $\mathbf{M}_t$ in the proposed methods equals to $\mathbf{\Sigma}_A$ matrix representing the noise distribution of the accelerometer and it is always diagonal. Therefore, divergence problems of KF process would be out of the question.

4.2 Adaptive Kalman Filtering with Noise Covariance Tuning

In this section, the problem of tuning the measurement noise covariance matrix is to be covered and two different adaptive tuning approaches, which have common background, are to be proposed. Theoretical background behind both the proposed algorithms is performing an innovation based adaptive tuning for the measurement noise covariance matrix. In line with the idea in our recent work [43], the method relies on comparison of the theoretical and real values of the innovation covariance. Therefore, when external acceleration exists, the filter can adapt itself to this new environment. Innovation in KF structure was defined at (4.1) and if there exist mismatches between the process and measurement models, due to the unaccounted external accelerations, KF gain changes with varying innovation covariance that can be represented as,

$$\hat{\mathbf{C}}_{e_t} = \mathbf{H}\mathbf{P}_t^-\mathbf{H}^T + \hat{\mathbf{\Sigma}}_{acc} + \mathbf{\Sigma}_A, \tag{4.10}$$

and KF gain becomes,

$$\mathbf{K}_t = \mathbf{P}_t^- \mathbf{H}^T (\mathbf{H}\mathbf{P}_t^- \mathbf{H}^T + \hat{\mathbf{\Sigma}}_{acc} + \mathbf{\Sigma}_A)^{-1}, \tag{4.11}$$

where $\mathbf{P}_t^-$ is the predicted covariance matrix during the KF process and $\hat{\mathbf{\Sigma}}_{acc}$ is the estimate for $\mathbf{\Sigma}_{acc}$ matrix given in (4.11). The real innovation covariance $\hat{\mathbf{C}}_{e_t}$ is to be presented individually for the proposed two approaches. It is the fact that, in steady-state, if the real value of error for an optimally running KF exceeds the theoretical error as,

$$tr(\mathbf{e}_t \mathbf{e}_t^T) \geq tr(\mathbf{H}\mathbf{P}_t^- \mathbf{H}^T + \hat{\mathbf{\Sigma}}_{acc} + \mathbf{\Sigma}_A), \tag{4.12}$$

there is external acceleration and the filtering process must be executed adaptively. In (4.12), $tr(.)$ denotes that the trace of the matrix. Only the real innovation covariance at time t is considered to be able to detect the instantaneous variations in the external acceleration. There are two possible options for tuning the measurement covariance matrix, STF and MTF options, respectively. These two different approaches with a novel perspective are to be proposed and explained next.

For both approaches the common frame of the algorithm is similar and presented in the Figure 4.2. Calculation of $\mathbf{\Sigma}_{acc}$ differs in two approaches as will be explained.

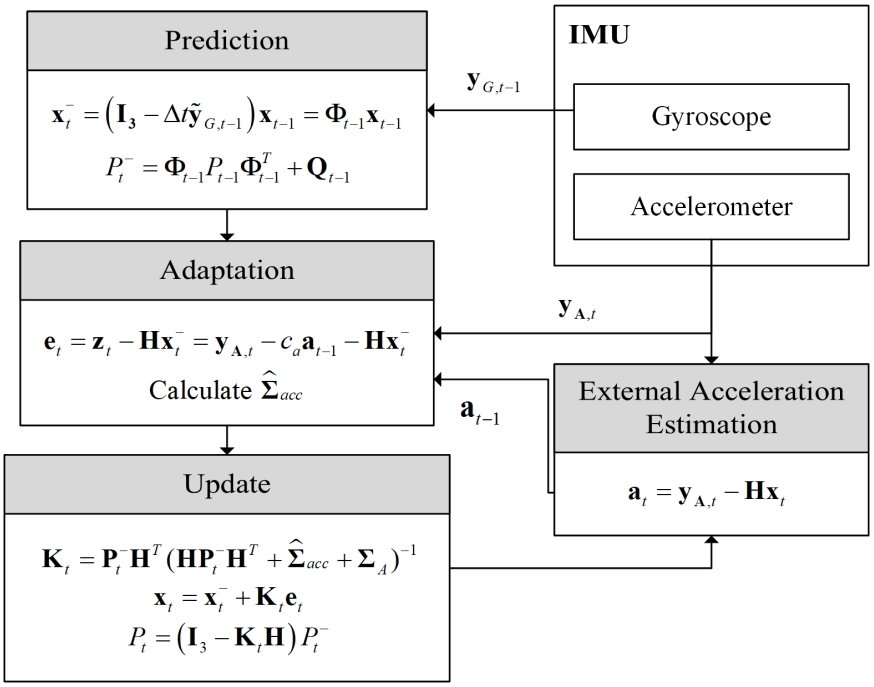

Figure 4.2: Common frame for the proposed RKF with tuning algorithms

4.2.1 Single-Tuning Factor Method

In the first approach, compensating the external acceleration in all three-axes equally is considered and the $\hat{\mathbf{\Sigma}}_{acc}$ matrix is estimated as a matrix whose diagonals are all equal and tuned with a STF. Denoting this STF as S_t, first let us write the Kalman gain as,

$$\mathbf{K}_t = \mathbf{P}_t^- \mathbf{H}^T (\mathbf{H}\mathbf{P}_t^- \mathbf{H}^T + S_t \mathbf{I_3} + \mathbf{\Sigma}_A)^{-1}. \tag{4.13}$$

In this case, by representing the real innovation covariance as $\hat{\boldsymbol{C}}_{e_t} = \boldsymbol{e}_t \boldsymbol{e}_t^T$, (4.10) can be rewritten as,

$$\mathbf{e}_t \mathbf{e}_t^T = \mathbf{H}\mathbf{P}_t^- \mathbf{H}^T + S_t \mathbf{I_3} + \mathbf{\Sigma}_A, \tag{4.14}$$

having trace of both side of the equation gives,

$$\mathbf{e}_t^T \mathbf{e}_t = tr\left\{\mathbf{H}_t \mathbf{P}_t^- \mathbf{H}_t^T\right\} + \mathbf{3}S_t + tr\left\{\mathbf{\Sigma}_A\right\}. \tag{4.15}$$

Then the STF to be used for this approach becomes,

$$S_t = \frac{\mathbf{e}_t^T \mathbf{e}_t - tr\left\{\mathbf{H}_t \mathbf{P}_t^- \mathbf{H}_t^T\right\} - tr\left\{\mathbf{\Sigma}_A\right\}}{3}. \tag{4.16}$$

Therefore, the RKF with STF approach is able to perform the gain correction for the KF adaptively in case of any external acceleration by defining the estimated covariance matrix as $\hat{\mathbf{\Sigma}}_{acc} = S_t \mathbf{I_3}$. If the inequality condition mentioned in (4.12) is met, then S_t and innovation covariance automatically increase resulting with smaller Kalman gain. Thus, smaller gain improves the attitude estimation quality via reducing the effect of the external accelerations. In all other cases when the inequality (4.12) does not hold, the filter is assumed to operate optimally, so there is no need to introduce an additional measurement covariance $\hat{\mathbf{\Sigma}}_{acc}$. In this case, and also when the algorithm returns a negative value of S_t, implying negative covariance, which has no physical significance, the STF is simply set as $S_t = 0$. Despite proposing a straightforward solution to reflect the covariance of the unaccounted modeling errors into the Kalman gain, the STF approach tunes the covariance with a single factor by ignoring any uneven external acceleration that might be experienced in three axes. To solve this problem, next, we propose another tuning approach with MTFs.

4.2.2 Multiple-Tuning Factor Method

In the second approach, the MTF methodology is introduced with same modifications defined in previous approach. However, rather than to adaptively tune the Kalman gain via scalar factor, it becomes appropriate to use a matrix structure with multiple factors since STF approach rejects the measurements from all channels, even if the external acceleration is sensed in one direction. Nevertheless, MTF approach only disregards the measurements of the axis in which external acceleration is sensed. In this case, by also redefining the innovation covariance as,

$$\hat{\mathbf{C}}_{e_t} = \frac{1}{\mu} \sum_{j=k-\mu+1}^{k} \mathbf{e}_j \mathbf{e}_j^T, \tag{4.17}$$

(4.11) can be rewritten to give the condition for estimating the $\hat{\mathbf{\Sigma}}_{acc}$ matrix,

$$\frac{1}{\mu} \sum_{j=k-\mu+1}^{k} \mathbf{e}_j \mathbf{e}_j^T = \mathbf{H}\mathbf{P}_t^- \mathbf{H}^T + \mathbf{S}_t + \mathbf{\Sigma}_A. \tag{4.18}$$

Here $\mathbf{S}_t$ is the tuning matrix composed of MTFs and μ defines the size of the moving window for innovation covariance calculation. By rearranging we can have the tuning matrix as,

$$\mathbf{S}_t = \frac{1}{\mu} \sum_{j=k-\mu+1}^{k} \mathbf{e}_j \mathbf{e}_j^T - \mathbf{H}_t \mathbf{P}_t^- \mathbf{H}_t^T - \mathbf{\Sigma}_A. \tag{4.19}$$

Therefore, RKF with MTF approach is able to perform the optimal correction as STF does, but with an improved way since multiple factors are used. Element/s of $\mathbf{S}_t$,which correspond to the axes with external acceleration, adapt itself if the inequality condition mentioned in (4.12) is met, and this provides efficient tuning procedure for the measurement noise covariance matrix. It should be emphasized that,

- Rather than using directly the $\mathbf{S}_t$ matrix as the covariance estimate, having the diagonal elements is required since there is no assumed correlation in between the external accelerations (and modeling errors) sensed in each axis.
- A negative covariance value does not have physical significance, so if the estimation result is negative, setting the estimate to 0 is necessary.

Thus the final estimate for $\hat{\mathbf{\Sigma}}_{acc}$ can be obtained as,

$$\hat{\mathbf{\Sigma}}_{acc} = diag(s_1, s_2, s_3), \tag{4.20}$$

$$s_i = max\left\{0, \mathbf{S}_{ii}\right\}, i = 1, 2, 3. \tag{4.21}$$

Here, $\mathbf{S}_{ii}$ represents the i^{th} diagonal element of the matrix $\mathbf{S}$. As mentioned, if the there is external acceleration, $\mathbf{S}$ changes the measurement noise covariance matrix and in all other cases, diagonal values are zero. Following section is to demonstrate the proposed methods and compare their results with those of a number of benchmark algorithms using the real-world datasets for MAVs.

CHAPTER 5

EXPERIMENTAL RESULTS

Results are given as the evaluation and performance comparison of the proposed adaptive KF methods including two different strategies with two different approaches and selected benchmark methods. In this case, there are experiment-based and simulation-based options for the extraction of the results. Since the experimental data represent the real-world better in terms of random and sudden external disturbances, in this thesis study, two notable experimental UAV datasets from the literature and the dataset for a ground vehicle retrieved from SAGE are used.

Detailed information about the dataset environment, experimental and instrumental setup used during the data collection can be found in the papers of these studies referenced in the following subsections. Attitude estimation is executed with the benchmark algorithms explained in the previous section and some basic algorithms excluded from this section due to absence of any adaptation against external disturbances. Excluded methods are gyroscope-only and accelerometer-only attitude estimation in which the attitude estimation problem is tried to be solved by only relying gyro and accelerometer measurements. Four different RKF method proposed in this thesis study are tested and evaluated. Moreover, rather than to estimate the attitude in 2D with the methods mentioned, Guo's and Dai's filters are implemented into the study for 3D attitude estimation with the magnetometer measurements. Magnetometer measurements are created by using IGRF and these filters are executed for estimating the attitude in 3D. The reason why to add these two full attitude filters is that to see even though the magnetometer measurements are taken into account, the estimation performance cannot surpass the proposed RKF algorithms in existence of the external acceleration and disturbances during the motion.

5.1 The Zurich Urban MAV Dataset Results

Provided by Majdik et al from University of Zurich, the dataset is collected with a camera equipped MAV that was flown within urban areas of Zurich at low altitudes. The 2 km dataset includes time synchronized aerial high-resolution images, global positioning system, GPS and IMU sensor data, ground-level street view images, and ground truth data that makes this dataset is suitable for navigation studies [44]. Table 5.1 demonstrates the attitude estimation results on this specific dataset.

Table 5.1: Attitude Estimation Results on Zurich MAV Dataset

Methods	**Roll RMSE** (°)	**Pitch RMSE** (°)
Gyroscope-Only	69.0203	34.8541
Accelerometer-Only	3.3078	2.2880
Mahony's Filter	1.0216	0.9231
Madgwick's Filter	1.6038	1.2753
Lee's Filter	0.9795	0.9152
Harada's Filter	2.3409	2.1916
Guo's Filter	2.3651	1.9623
Dai's Filter	2.3441	1.9134
Standard KF (S_t=0)	3.0872	2.1149
RKF (SSF) / Approach 1	**1.2256**	**1.2117**
RKF (MSF) / Approach 2	**0.6700**	**0.5764**
RKF (STF) / Approach 1	**0.6741**	**0.5805**
RKF (MTF) / Approach 2	**0.5437**	**0.4627**

Obviously, the performance of the proposed method with its scaling approach, i.e. RKF with MSF is slightly improving the estimation quality of the KF-based Lee's filter. Nevertheless, the accuracy of the proposed method with its second tuning approach (RKF with MTF) is superior against all of the benchmark algorithms, even Lee's filter, which is one of the widely accepted and reliable solutions for attitude estimation problem. Figure 5.1, 5.2, 5.3 and 5.4 visually demonstrate the estimation performance of the proposed RKF algorithms with respect to Lee's filter.

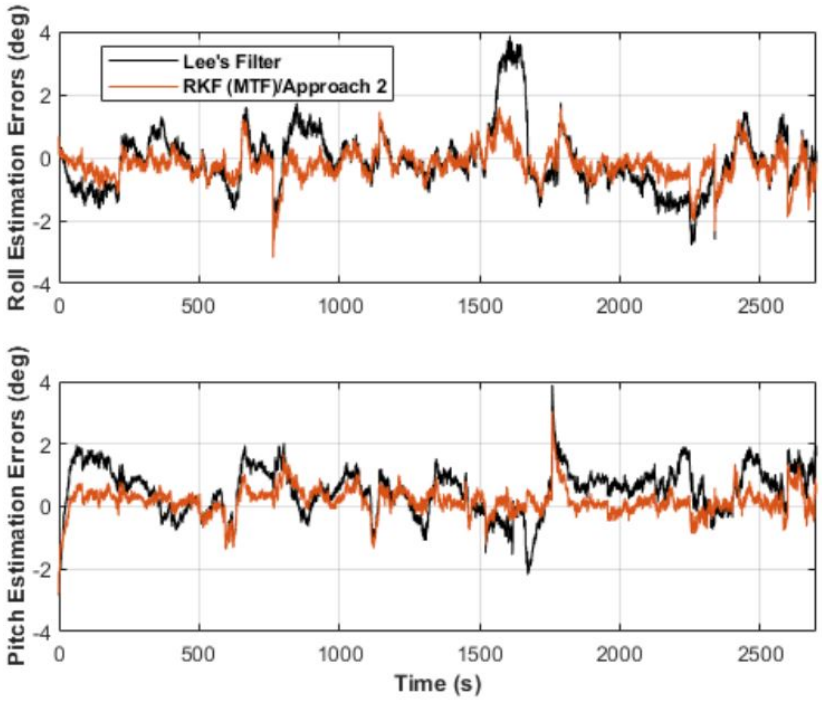

Figure 5.1: Roll and pitch angle estimation errors for the Zurich MAV dataset for RKF with MTF

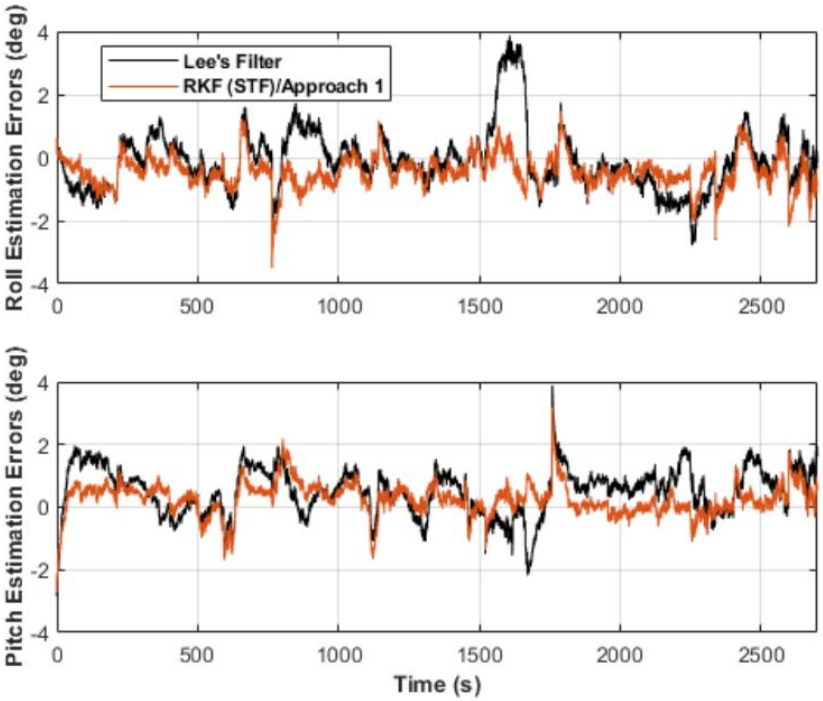

Figure 5.2: Roll and pitch angle estimation errors for the Zurich MAV dataset for RKF with STF

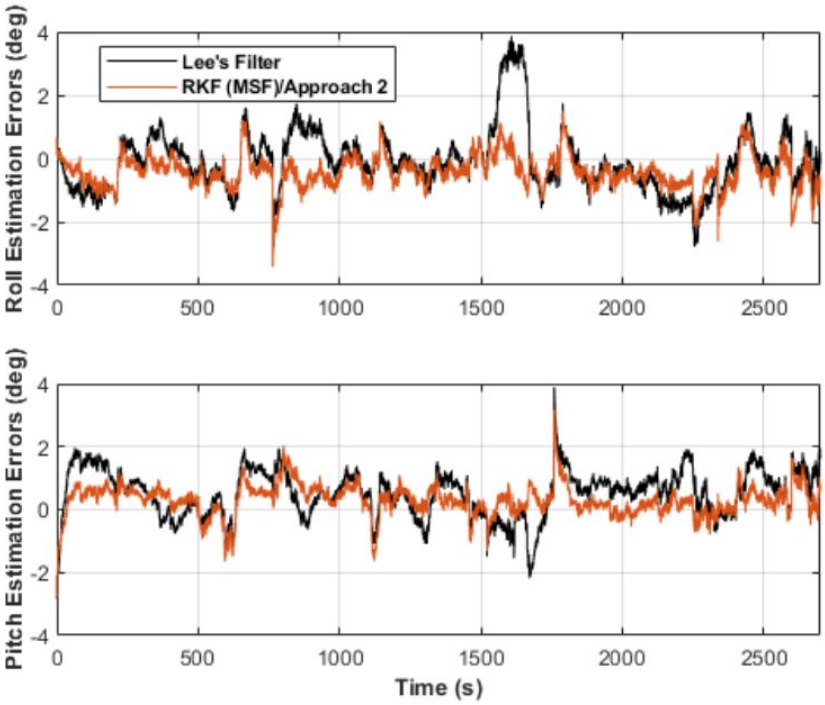

Figure 5.3: Roll and pitch angle estimation errors for the Zurich MAV dataset for RKF with MSF

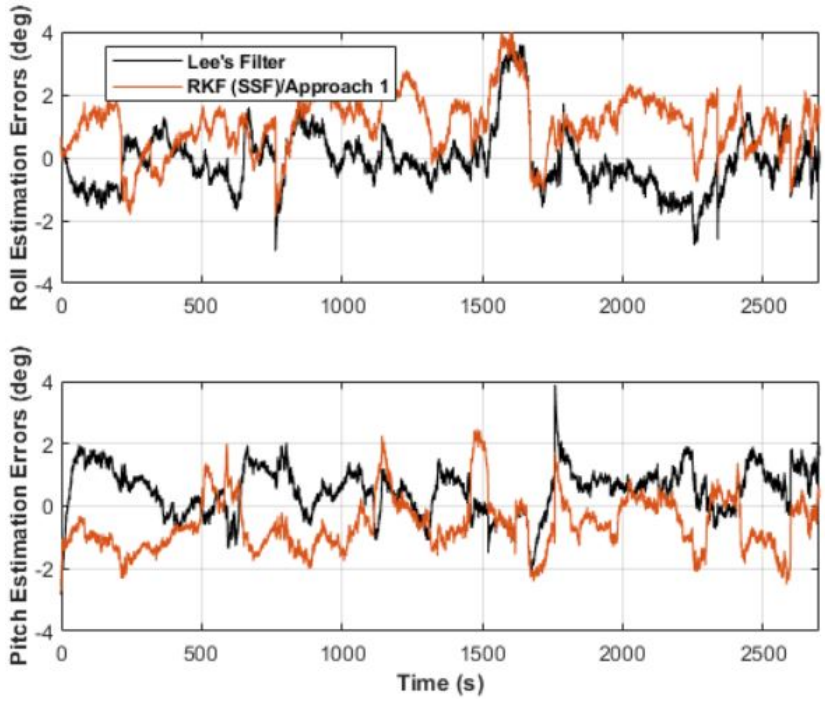

Figure 5.4: Roll and pitch angle estimation errors for the Zurich MAV dataset for RKF with SSF

The reason behind this superior performance in terms of the attitude estimation accuracy is basically the capability of the filters for representing the measurement noise covariances more accurately whenever the platform is subjected to the external accelerations during the motion. Better construction of the measurement noise covariance matrix via using multiple factors in case of acceleration and the accurate compensation of external accelerations improve the attitude estimation performance during the filtering process. This is a feature that Lee's filter cannot provide using (3.40) as the covariance for external accelerations. Standard KF (where $S_t = 0$) is less accurate than the Lee's filter as it does not apply any covariance correction for external accelerations. Harada's filter, on the other hand, can estimate the attitude better than the standard KF in this scenario by completely ignoring the measurements when the external acceleration is detected. The RKF with SSF, MSF and STF can increase the accuracy with a better representation of the covariance compared to (3.40), but falls behind the RKF with MTF as using STF ignores all measurements regardless of the actual direction that the platform is accelerating.

5.2 EuRoC MAV Dataset Results

EuRoC visual-inertial dataset is collected on board a MAV that was flown on an industrial machine hall and Vicon room that is specially designed for localization studies. The dataset includes synchronized stereo images, IMU measurements and accurate 6D ground truth pose and in this work, machine hall datasets are used in which the ground truth values are extracted by simultaneous localization and mapping algorithms [45]. Note that, this dataset is for different motion profiles including relatively higher external accelerations and more agile maneuvers than the Zurich MAV dataset. Ranging from slow flights in a small, cluttered workspace to dynamic flights in a large hall, EuRoC MAV dataset allows evaluating the algorithms in various flight conditions. Readers may refer to these studies for the details of the datasets, calibration procedure and ground truth evaluation. For all evaluations the process noise covariance matrix and Σ_A part of the measurement noise covariance matrix are set in accordance with the sensor specifications. Table 5.2, 5.3 and 5.4 are given in order to show the attitude estimation results for these dataset.

Table 5.2: Attitude Estimation Results on EuRoC MAV Dataset (Machine Hall 01)

Methods	**Roll RMSE** (°)	**Pitch RMSE** (°)
Mahony's Filter	7.0809	2.4944
Madgwick's Filter	7.0607	2.3238
Lee's Filter	1.6999	1.3085
Harada's Filter	1.8993	1.4014
Guo's Filter	2.7652	1.6617
Dai's Filter	2.5241	1.6143
Standard KF (S_t=0)	3.4809	1.8592
RKF (SSF) / Approach 1	**1.2256**	**1.2117**
RKF (MSF) / Approach 2	**1.1529**	**1.2070**
RKF (STF) / Approach 1	**1.2211**	**1.1436**
RKF (MTF) / Approach 2	**1.0629**	**1.1783**

Table 5.3: Attitude Estimation Results on EuRoC MAV Dataset (Machine Hall 02)

Methods	**Roll RMSE** (°)	**Pitch RMSE** (°)
Mahony's Filter	6.1953	2.3371
Madgwick's Filter	8.9748	3.1815
Lee's Filter	1.7447	0.8074
Harada's Filter	2.9069	1.2201
Guo's Filter	2.3651	1.9623
Dai's Filter	2.3441	1.9123
Standard KF (S_t=0)	2.3350	0.9962
RKF (SSF) / Approach 1	**1.2256**	**1.2117**
RKF (MSF) / Approach 2	**1.1805**	**0.5312**
RKF (STF) / Approach 1	**1.2565**	**0.5156**
RKF (MTF) / Approach 2	**1.1940**	**0.4973**

Table 5.4: Attitude Estimation Results on EuRoC MAV Dataset (Machine Hall 05)

Methods	**Roll RMSE** (°)	**Pitch RMSE** (°)
Mahony's Filter	5.6700	2.1121
Madgwick's Filter	6.9964	2.3728
Lee's Filter	2.1221	0.9282
Harada's Filter	4.7355	1.4126
Guo's Filter	2.3651	1.9623
Dai's Filter	2.3441	1.9123
Standard KF (S_t=0)	2.4533	1.9092
RKF (SSF) / Approach 1	**1.2256**	**1.2117**
RKF (MSF) / Approach 2	**1.1529**	**1.2070**
RKF (STF) / Approach 1	**1.8415**	**0.4714**
RKF (MTF) / Approach 2	**0.8823**	**0.4021**

Note that three individual dataset with increasing motion complexity are used in attitude estimation process. As to the Lee's filter, RKFs provide accurate estimates compared to other benchmark algorithms in all other cases. In the end, its accuracy depends on how well the Σ_{acc} can be represented for the actual acceleration profile that the platform is experiencing. Depending on the acceleration profile, Harada's filter may provide less accurate results even compared to the standard KF, since it does not use the measurements at all when the acceleration is detected. The proposed RKFs, on the other hand, consistently assure the highest estimation accuracy. Even the STF approach brings about noteworthy improvement in the accuracy despite mapping all three channel accelerations to a STF, which has deficiencies in practice as discussed. Together with the results in Tables 5.2, 5.3 and 5.4, it becomes clear that the performance of the CFs deteriorate due to the existence of highly dynamic scenarios whereas KF-based Lee's filter shows the best performance among the benchmark algorithms. Moreover, Figure 5.5-5.8 visually demonstrate (for Machine Hall 05 dataset) that the proposed RKF algorithms, compared to Lee's KF, achieves better accuracy during the whole flight course of the MAV.

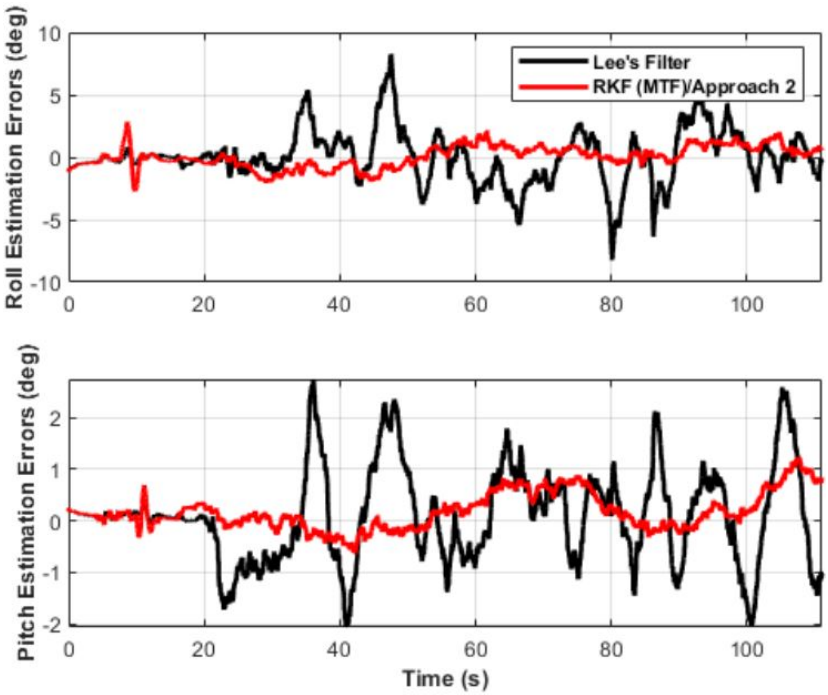

Figure 5.5: Attitude angles estimation errors for the EuRoC MAV dataset for RKF with MTF (Machine Hall 05)

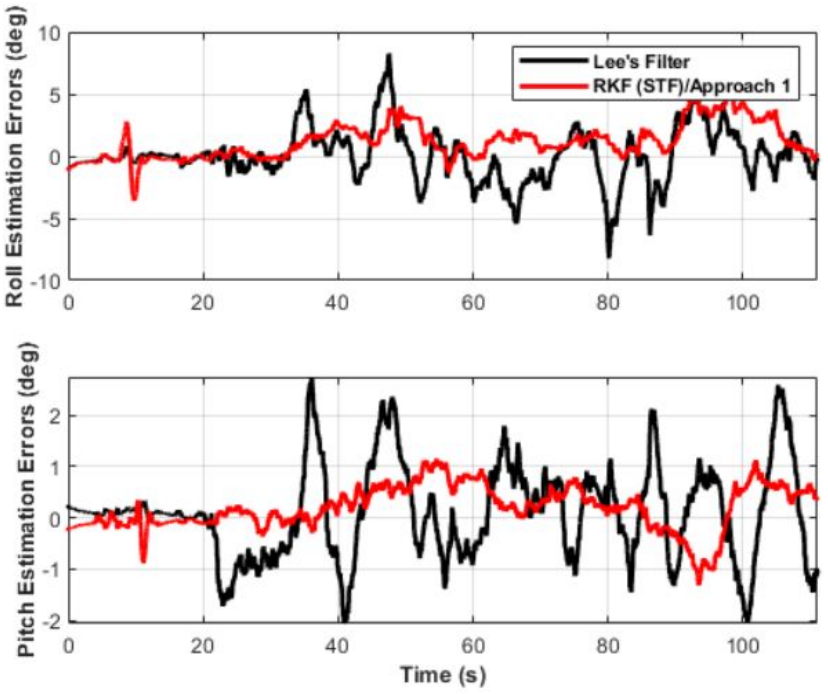

Figure 5.6: Attitude angles estimation errors for the EuRoC MAV dataset for RKF with STF (Machine Hall 05)

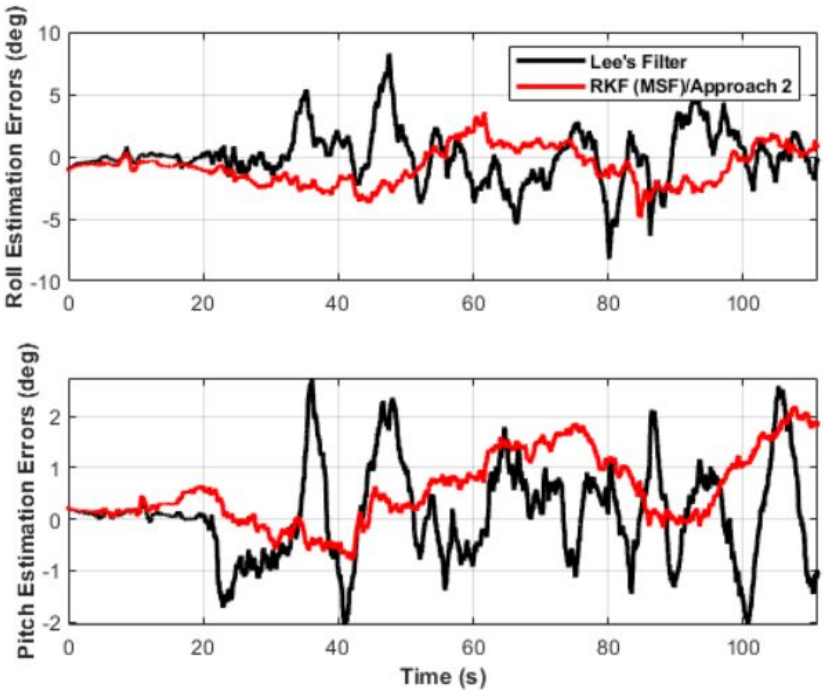

Figure 5.7: Attitude angles estimation errors for the EuRoC MAV dataset for RKF with MSF (Machine Hall 05)

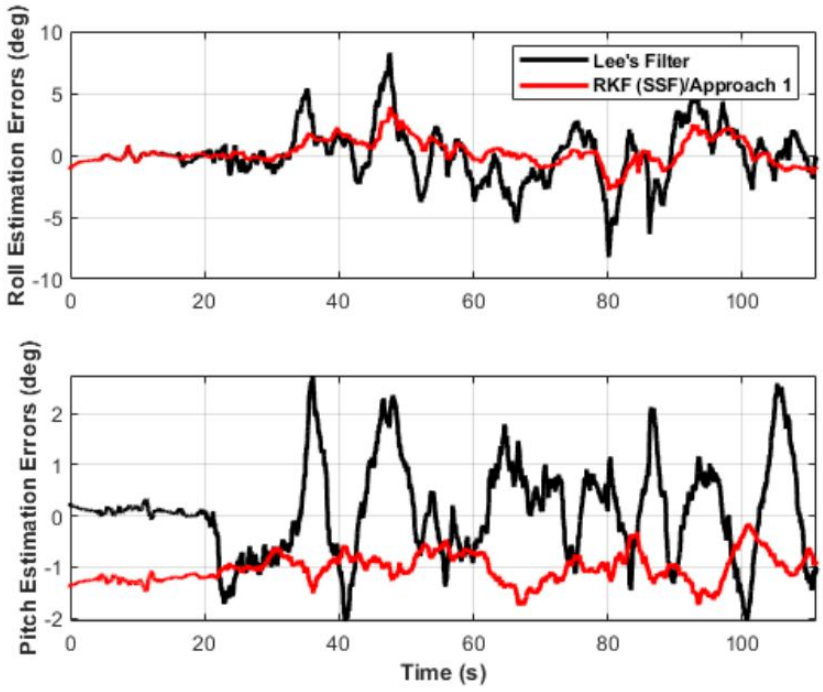

Figure 5.8: Attitude angles estimation errors for the EuRoC MAV dataset for RKF with SSF (Machine Hall 05)

As seen from the Figure 5.5-5.8, the RKF with MTF, compared to Lee's KF, achieves better accuracy in terms of attitude estimation during the whole flight course of the MAV. Occasionally, the attitude estimation error for Lee's filter increases and becomes as large as 8°. However, the error for RKF with MTF is within the $\pm 2°$ and $\pm 1°$ bounds for roll and pitch angles, respectively, throughout the whole duration. Moreover, Figure 5.9 visualizes the MTFs and the sensed external accelerations in all three sensor axes in this scenario. External acceleration is computed by subtracting the gravity vector in the body frame, which is obtained using the true orientation, from the accelerometer measurements. Compensation effect of adaptation by means of variations in the MTFs can be clearly seen especially after the 20th second.

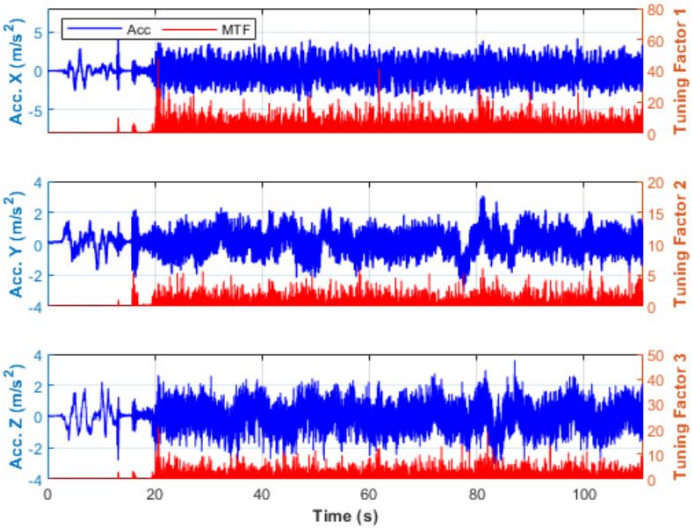

Figure 5.9: External acceleration profile during the motion and response of tuning factors (EuRoC Machine Hall 05)

Moreover, it is important to see whether the filter works efficiently and without any problems. Therefore, Figure 5.10, 5.11 and 5.12 are given in order to show the error residuals (variation between filter estimations and real values) for the states during the estimation process is within the 3σ boundaries of the error covariance matrix. Finally, Figure 5.13 demonstrates the effects of different c_a values, the cutoff frequency of the low-pass filter for external accelerations, on the accuracy of the algorithm. Results are compared with those of Lee's filter, which depends on the set c_a values for external acceleration compensation. For the whole spectrum of c_a values, the RKF with MTF repeatedly prevails in terms of accuracy.

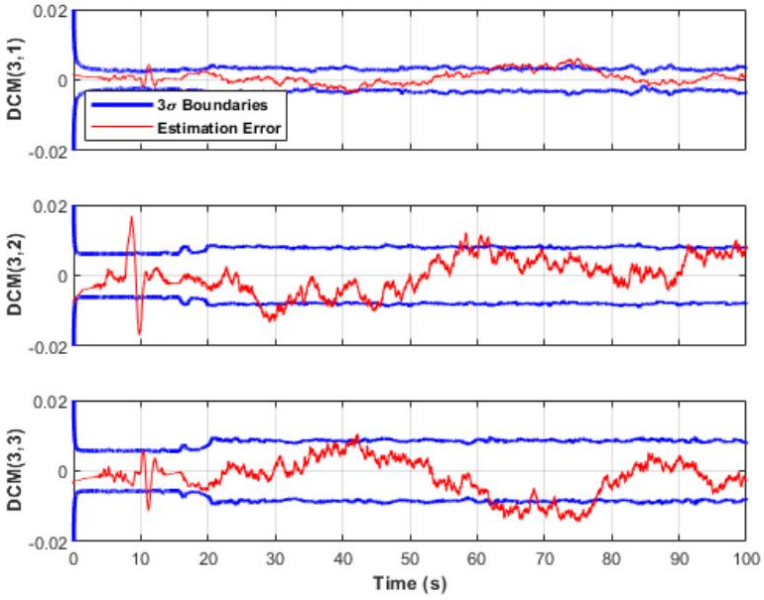

Figure 5.10: Estimation error and 3σ error boundaries for RKF with MTF

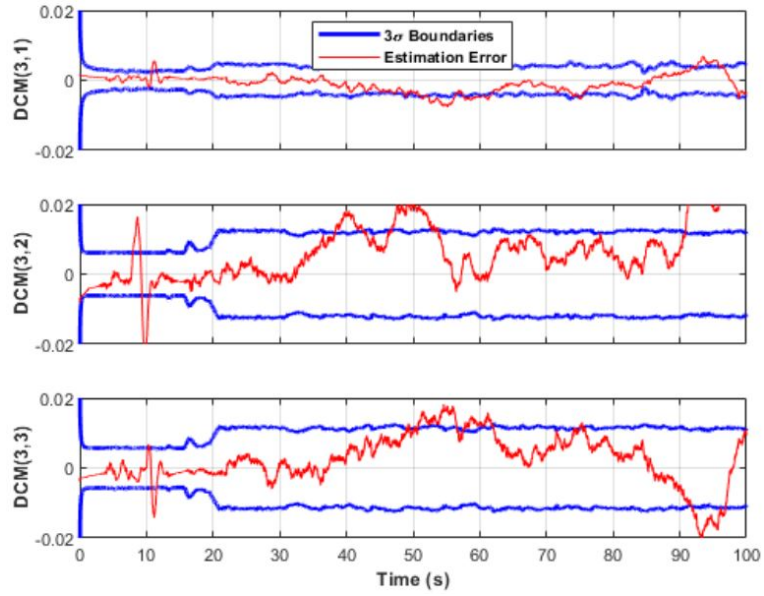

Figure 5.11: Estimation error and 3σ error boundaries for RKF with STF

It is observed from the Figure 5.10-5.11 that the proposed algorithms with tuning approach demonstrate enhanced performance in terms of the estimation performance with respect to Lee's filter given on Figure 5.12. Lee's filter cannot squeeze the estimation error within the 3σ boundaries due to its inefficiency for setting the optimal measurement noise covariance matrix during the disturbed and accelerated motion.

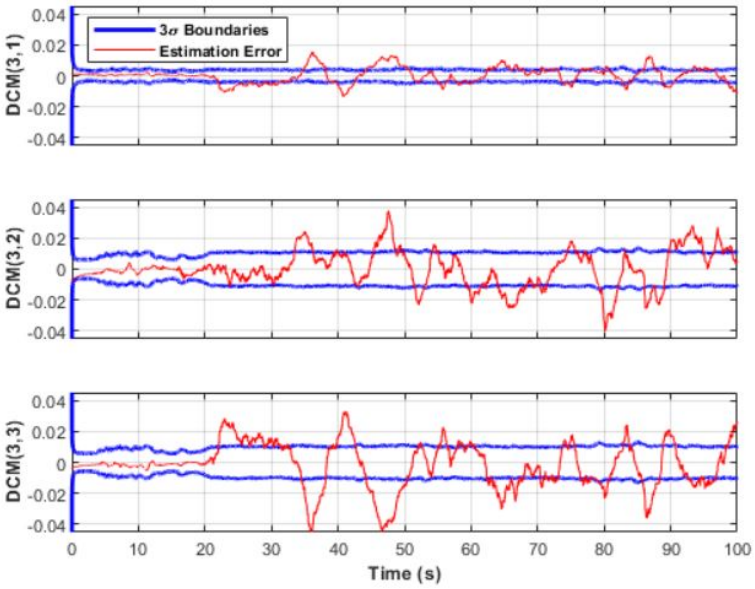

Figure 5.12: Estimation error and 3σ error boundaries for Lee's filter

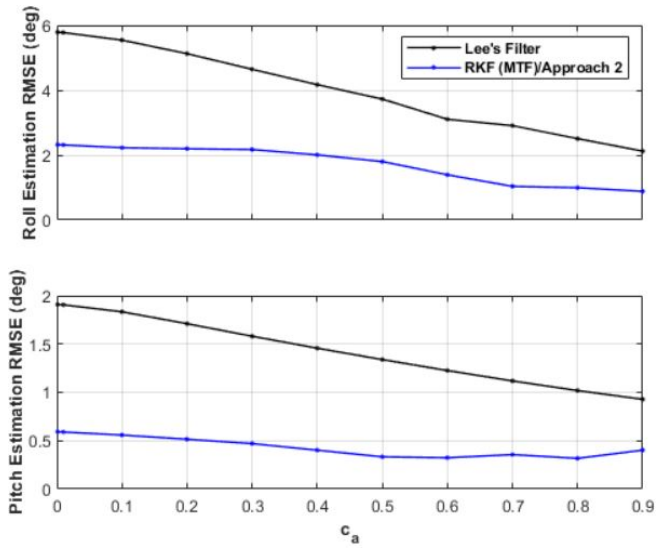

Figure 5.13: Comparison of filter accuracies for different cutoff frequency constant (c_a) values (EuRoC Machine Hall 05)

As expected, while the cut-off frequency is lowered such that the external accelerations are not low-pass filtered, the accuracy gap in between two filters increases. Specifically for this dataset, Lee's filter works better only if the oscillations in the external accelerations can be filtered out with larger c_a values. Even in this case the RKF with MTF is almost two times more accurate as already discussed.

Table 5.5: Algorithm Execution Time of Each Filter for Zurich MAV Dataset over 100 Independent Runs

Method	**Madgwick's Filter**	**Mahony's Filter**	**Lee's Filter**	**Harada's Filter**	**Guo's Filter**	**Dai's Filter**
Average Execution Time (s)	0.683	0.546	1.244	1.251	1.267	1.289
Method	**Standard KF**	**RKF (SSF)**	**RKF (MSF)**	**RKF (STF)**	**RKF (MTF)**	
Average Execution Time (s)	1.244	1.244	1.246	1.245	1.247	

The computational load of the proposed algorithms and the benchmark methods are evaluated via storing their run times for 100 different runs. The computational performance evaluation is done for Zurich Urban MAV dataset on a computer with specifications Intel Core i-7, 2.20GHz, 16GB RAM using MATLAB version R2020b. Table 5.5 summarizes the results in terms of average execution times. More or less all the KF structured algorithms require similar run times while required time for the CF algorithms, denoted as simpler and computationally efficient, is below under the average time for KF algorithms [24]. However, it is important to note that Dai's and Guo's filter are the most sluggish between the competitors since these algorithms are full attitude filters and also take the magnetometer measurements into account.

Before to conclude the results for EuRoC MAV dataset, it is also appropriate to mention the effect of the tuning factors. The one might think that the maximum value of multiple tuning factors can be chosen during the whole filtering procedure for better compensation. In this context, for EuRoC 05 dataset, maximum values of tuning factors are obtained and the diagonals of $\mathbf{S}_t$ are set as these values. This methodology will be called as RKF ($\mathbf{S}_{max}$) and results on Table 5.6 shows the performance comparison between RKF (MTF) and RKF ($\mathbf{S}_{max}$) strategies in terms of attitude estimation RMSE.

Table 5.6: The Effect of Constant Maximum Tuning Factors over Estimation Results

Methods	**Roll RMSE (°)**	**Pitch RMSE (°)**
RKF (MTF) / Approach 2	**0.8823**	**0.4021**
RKF ($\mathbf{S}_{max}$) Approach	**2.3776**	**1.2694**

Figure 5.14 shows the visual representation of this performance comparison between these two methods.

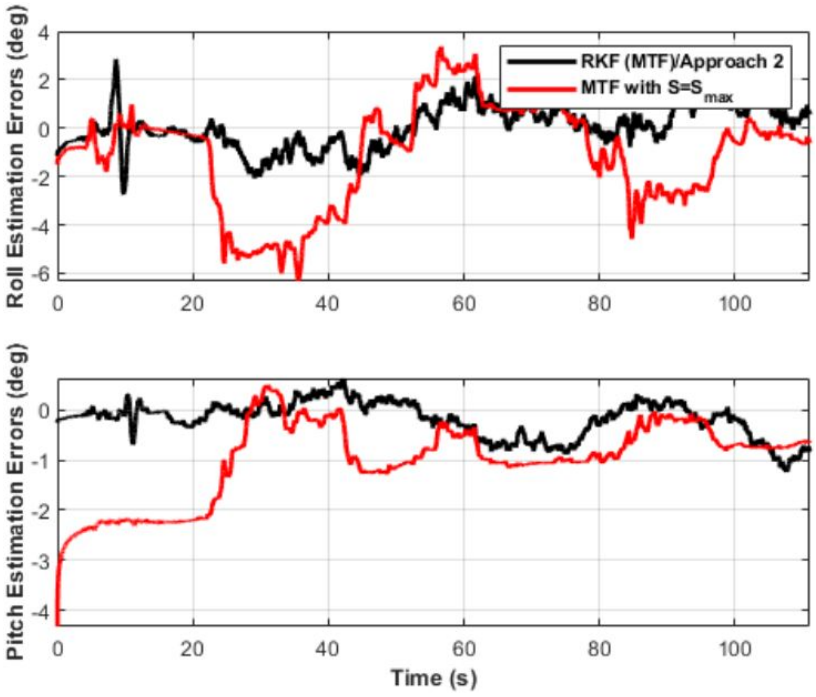

Figure 5.14: Estimation error and 3σ error boundaries for Lee's filter

Even though intuitions might be the tuning matrix with the constant maximum tuning factors is able to compensate external accelerations via smaller Kalman gain during whole flight. However, as observed from Table 5.6 and Figure 5.14, $\mathbf{S}_{max}$ approach shows no improvement and the performance of this method is very poor when to be compared with RKF (MTF) approach. The reason why this low-performance is basically the non-existence of any online adaptation, which MTF method can execute. These results indicate the proposed MTF methodology with online adaptation of $\mathbf{S}_t$ is better than $\mathbf{S}_{max}$ strategy in terms of the attitude estimation quality.

5.3 TUBITAK SAGE Dataset Results

The experimental dataset used in this study is retrieved from TUBITAK SAGE for the sake of this thesis study. It includes the accelerometer, with a velocity random walk value of ($< 50\mu g/\sqrt{Hz}$) and gyroscope, with an angular walk value of

($< 0.002°/\sqrt{h}$), measurements from a navigational grade inertial measurement unit which provides to test the proposed algorithms not only commercial and tactical grade IMUs but also in different IMU platforms. The experiment was conducted with the land vehicle on the rural area of Ankara, IMU data is collected on-board and the 6-DoF ground truth is obtained via GPS/INS solution. It is important to emphasize that the sampling rate of IMU is $512Hz$ while GPS/INS solution, i.e. reference orientation is obtained with $200Hz$. So, applying the different filter configurations from the benchmark methods mentioned previously and novel Kalman filter approaches, following results are obtained as seen on Table 5.7.

Table 5.7: Attitude Estimation Results on TUBITAK SAGE Dataset

Methods	**Roll RMSE** (°)	**Pitch RMSE** (°)
Gyroscope-Only	23.6548	21.2391
Accelerometer-Only	16.7451	12.3572
Mahony's Filter	6.4713	4.3128
Madgwick's Filter	3.9964	2.4715
Lee's Filter	0.1439	0.0969
Harada's Filter	0.1851	0.1137
Guo's Filter	0.1057	0.0641
Dai's Filter	0.1242	0.0734
Standard KF (S_t=0)	0.2531	0.2097
RKF (SSF) / Approach 1	**0.0312**	**0.1045**
RKF (MSF) / Approach 2	**0.0214**	**0.0093**
RKF (STF) / Approach 1	**0.0216**	**0.0089**
RKF (MTF) / Approach 2	**0.0210**	**0.0088**

Moreover, Figure 5.15 and 5.16 visually demonstrate that the RKF with two tuning approaches, compared to Lee's KF, achieves better accuracy in terms of attitude estimation quality both for the pitch and roll angles during the whole drive course of the land vehicle.

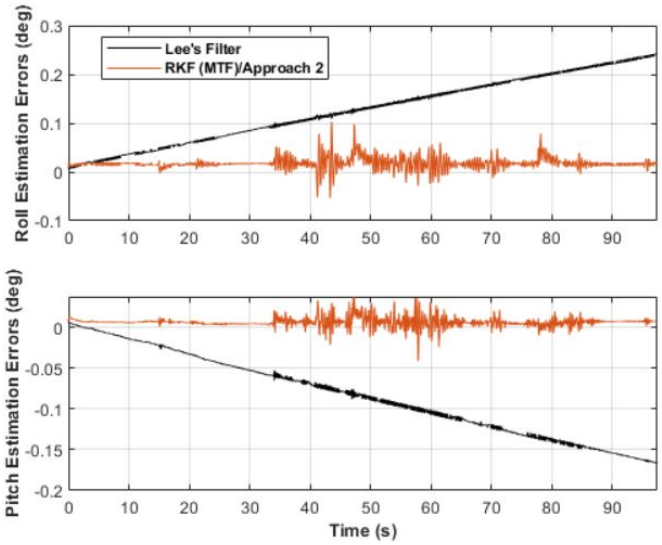

Figure 5.15: Attitude angles estimation errors for SAGE dataset for RKF with MTF

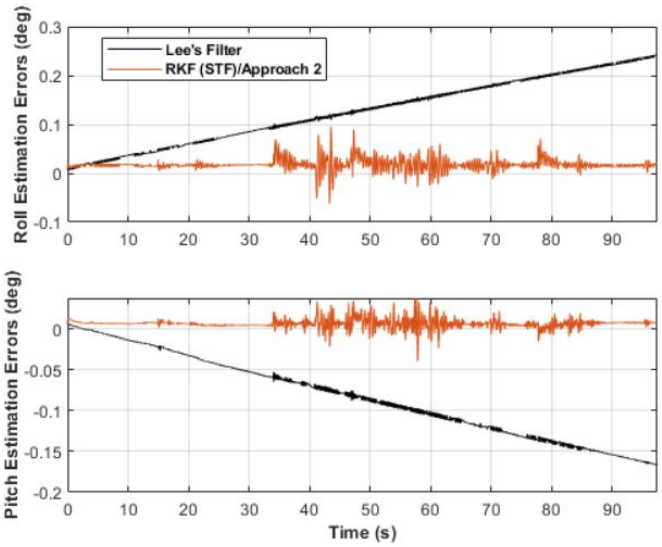

Figure 5.16: Attitude angles estimation errors for SAGE dataset for RKF with STF

As can be observed from the Figure 5.15-5.16, Lee's KF is not able to compensate highly dynamic external disturbances along the prolonged scenario and estimation accuracy deteriorates as time passes. RKF algorithms show better performance in both angle estimations and RKF with MTF performs superior performance against all of the methods. It is able to lower the negative side effects of the external disturbance via accurately compensating those in the filtering architecture and estimation error is not deteriorating but bounded within a small interval.

Figure 5.17 visualizes the MTFs and the sensed external accelerations in all three sensor axes in this scenario.

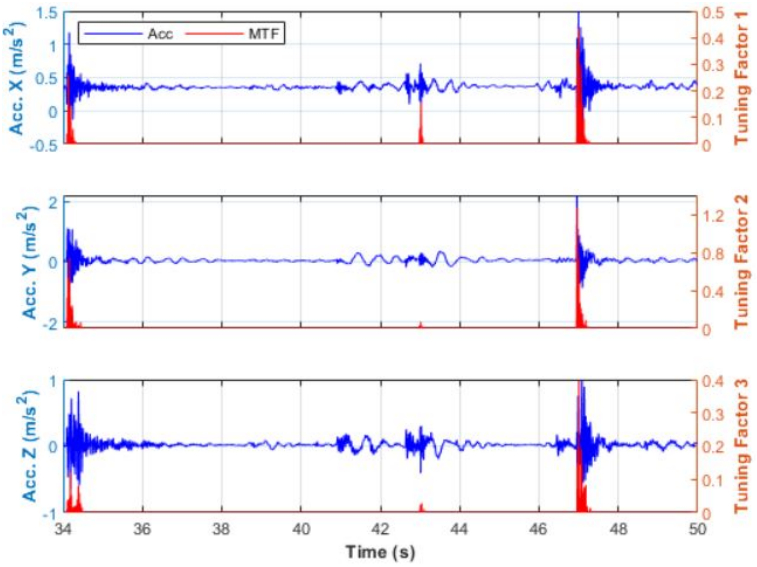

Figure 5.17: External acceleration profile during the motion and response of tuning factors (TUBITAK SAGE Dataset)

CHAPTER 6

CONCLUSION

In this thesis study, novel RKF algorithms are proposed for estimating the attitude only using the IMU measurements. The performance of the proposed methods in terms of the estimation quality are evaluated using real-world datasets and compared with the methods selected from the current literature. In the first part, a detailed introduction to the attitude determination with IMU and recent works in the literature are given. The fundamentals and theoretical background about the attitude determination problem are provided for the sake of future sections of this study. Then, the attitude estimation methodologies, proving their performances on IMU-only attitude determination, are selected from the literature. Finally, evaluation and performance comparison of the proposed methods including two different strategies with two different approaches are provided.

Results extracted via using real-world datasets show that when the dataset scenarios include prolonged and high external accelerations with other disturbances, KF-based algorithms designed for to compensate those disturbances in the literature exhibit gradually increasing estimation errors. These algorithms set initial adaptation for the measurement noise covariance matrix but do not make an online adaptation so that when unexpected, sudden disturbances occur, the estimation accuracy starts to deteriorate. Similar reasons apply for CFs during the estimation process. The scaling factor strategy with its single and multiple scaling approaches show just a slight improvement in the estimation accuracy against the benchmark methods. The reason why this accuracy cannot be improved much better is inefficient measurement noise covariance setting via scaling rather than tuning.

While in the tuning strategy, the first approach with single tuning factor slightly improves the estimation accuracy compared to benchmark KF-based filters and widely used complimentary filters, while the second approach with multiple tuning factors shows superior performance against all competitors. However, despite improving the accuracy, the RKF with STF cannot distinguish the external accelerations in different axes. On the other hand, the MTF approach can compensate the external accelerations in different axes individually and embodies a more effective way for adapting the KF.

Both algorithms incorporate a straightforward adaptation method, which has almost no extra computational demand and is easy to apply. However, full attitude filters such as Guo's and Dai's filters, designed for obtaining the orientation rather than the attitude, are more sluggish and do not enhance the estimation accuracy for the attitude which make them infeasible for IMU-only estimation.

Main focus on further investigations will be using the similar methods for estimating three-axis attitude, i.e. the full orientation for platforms including also the magnetometers and when the magnetometer measurements are corrupted with time-varying errors. In this manner, it is planned to design an adaptive multiplicative extended Kalman filter which would use a static attitude determination method such as TRIAD, QUEST or another alternative for combining the accelerometer and magnetometer measurements. Then, these refined measurements are fed into an adaptive MEKF architecture where the gyro measurements are used for propagating the states. Moreover, the effect of the same adaptations in orientation determination are to be investigated with advanced forms of Kalman filters such as UKF and CKF which are widely used for "capturing" the nonlinear dynamics of the states with weighted sampling points. Therefore, with those assumptions, it would also become possible to calibrate and compensate the errors of inertial and magnetic sensors.

The source codes are available on https://github.com/dukynuke/robustKFimuOnly for those who are interested. This website provides MATLAB scripts used in this thesis study.

REFERENCES

[1] A. Noureldin, T. Karamat, and J. Georgy, *Fundamentals of Inertial Navigation, Satellite-Based Positioning and Their Integration*, pp. 1–314. January 2013.

[2] M. Nazarahari and H. Rouhani, "40 years of sensor fusion for orientation tracking via magnetic and inertial measurement units: Methods, lessons learned, and future challenges," *Information Fusion*, vol. 68, pp. 67–84, 2021.

[3] M. Kok, J. D. Hol, and T. B. Schön, "Using inertial sensors for position and orientation estimation," *Foundations and Trends® in Signal Processing*, vol. 11, no. 1-2, pp. 1–153, 2017.

[4] G. Wahba, "A Least Squares Estimate of Satellite Attitude," *SIAM Review*, vol. 7, pp. 409–409, July 1965.

[5] P. B. Davenport, "A vector approach to the algebra of rotations with applications," 1968.

[6] H. D. Black, "A passive system for determining the attitude of a satellite," *AIAA Journal*, vol. 2, no. 7, pp. 1350–1351, 1964.

[7] M. D. Shuster and S. D. Oh, "Three-axis attitude determination from vector observations," *Journal of Guidance and Control*, vol. 4, pp. 70–77, Feb. 1981.

[8] L. F. Markley, "Attitude determination using vector observations and the singular value decomposition," *Journal of the Astronautical Sciences*, vol. 38, 11 1987.

[9] R. E. Kalman, "A new approach to linear filtering and prediction problems," *J. Basic Eng*, vol. 82, pp. 35–45, March 1960.

[10] A. Odry, I. Kecskes, P. Sarcevic, Z. Vizvari, A. Toth, and P. Odry, "A novel fuzzy-adaptive extended Kalman filter for real-time attitude estimation of mobile robots," *Sensors*, vol. 20, p. 803, February 2020.

[11] W. Youn, M. B. Rhudy, A. Cho, and H. Myung, "Fuzzy adaptive attitude estimation for a fixed-wing UAV with a virtual SSA sensor during a GPS outage," *IEEE Sensors Journal*, vol. 20, no. 3, pp. 1456–1472, 2020.

[12] M. B. Del Rosario, H. Khamis, P. Ngo, N. H. Lovell, and S. J. Redmond, "Computationally efficient adaptive error-state Kalman filter for attitude estimation," *IEEE Sensors Journal*, vol. 18, no. 22, pp. 9332–9342, 2018.

[13] F. Deng, H.-L. Yang, and L.-J. Wang, "Adaptive unscented Kalman filter based estimation and filtering for dynamic positioning with model uncertainties," *International Journal of Control, Automation and Systems*, vol. 17, 02 2019.

[14] A. C. B. Chiella, B. O. S. Teixeira, and G. A. S. Pereira, "Quaternion based robust attitude estimation using an adaptive unscented Kalman filter," *Sensors*, vol. 19, p. 2372, May 2019.

[15] S. Zihajehzadeh, D. Loh, T. J. Lee, R. Hoskinson, and E. J. Park, "A cascaded Kalman filter-based GPS/MEMS-IMU integration for sports applications," *Measurement*, vol. 73, pp. 200–210, September 2015.

[16] H. G. de Marina, F. J. Pereda, J. M. Giron-Sierra, and F. Espinosa, "UAV attitude estimation using unscented Kalman filter and TRIAD," *IEEE Transactions on Industrial Electronics*, vol. 59, no. 11, pp. 4465–4474, 2012.

[17] W. Sun, J. Wu, W. Ding, and S. Duan, "A robust indirect Kalman filter based on the gradient descent algorithm for attitude estimation during dynamic conditions," *IEEE Access*, vol. 8, pp. 96487–96494, 2020.

[18] J. Wu, "MARG attitude estimation using gradient-descent linear Kalman filter," *IEEE Transactions on Automation Science and Engineering*, vol. 17, no. 4, pp. 1777–1790, 2020.

[19] S. O. H. Madgwick, A. J. L. Harrison, and R. Vaidyanathan, "Estimation of IMU and MARG orientation using a gradient descent algorithm," in *Proc. IEEE Int. Conf. Rehabil. Robot.*, pp. 1–7, IEEE, June 2011.

[20] H. Fourati, N. Manamanni, L. Afilal, and Y. Handrich, "A nonlinear filtering approach for the attitude and dynamic body acceleration estimation based on

inertial and magnetic sensors: Bio-logging application," *IEEE Sensors Journal*, vol. 11, pp. 233–244, January 2011.

[21] H. Fourati, "Heterogeneous data fusion algorithm for pedestrian navigation via foot-mounted inertial measurement unit and complementary filter," *IEEE Trans. Instrum. Meas*, vol. 64, pp. 221–229, January 2015.

[22] J. Wu, Z. Zhou, B. Gao, R. Li, Y. Cheng, and H. Fourati, "Fast linear quaternion attitude estimator using vector observations," *IEEE Transactions on Automation Science and Engineering*, vol. 15, pp. 307–319, January 2018.

[23] E. R. Bachmann, R. B. McGhee, X. Yun, and M. J. Zyda, "Inertial and magnetic posture tracking for inserting humans into networked virtual environments," *Association for Computing Machinery*, pp. 9–16, 2001.

[24] M. A. Javed, M. Tahir, and K. Ali, "Cascaded Kalman filtering-based attitude and gyro bias estimation with efficient compensation of external accelerations," *IEEE Access*, vol. 8, pp. 50022–50035, 2020.

[25] R. Mahony, T. Hamel, and J.-M. Pflimlin, "Nonlinear complementary filters on the special orthogonal group," *IEEE Trans. Autom. Control*, vol. 53, pp. 1203–1218, June 2008.

[26] S. O. H. Madgwick, "An efficient orientation filter for inertial and inertial/magnetic sensor arrays," vol. 25, 2010.

[27] A. Cavallo, A. Cirillo, P. Cirillo, G. De Maria, P. Falco, C. Natale, and S. Pirozzi, "Experimental comparison of sensor fusion algorithms for attitude estimation," in *IFAC Proceedings Volumes (IFAC-PapersOnline)*, vol. 19, pp. 7585–7591, IFAC, 2014.

[28] M. Nowicki, J. Wietrzykowski, and P. Skrzypczynski, "Simplicity or flexibility? Complementary Filter vs. EKF for orientation estimation on mobile devices," *Proceedings - 2015 IEEE 2nd International Conference on Cybernetics, CYBCONF 2015*, pp. 166–171, 2015.

[29] R. G. Valenti, I. Dryanovski, and J. Xiao, "A linear Kalman filter for MARG orientation estimation using the algebraic quaternion algorithm," *in IEEE Trans-*

actions on Instrumentation and Measurement, vol. 65, pp. 467–481, February 2016.

[30] Z. Zhou, Y. Li, J. Liu, and G. Li, "Equality constrained robust measurement fusion for adaptive Kalman-filter-based heterogeneous multi-sensor navigation," *IEEE Transactions on Aerospace and Electronic Systems*, vol. 49, pp. 2146–2157, October 2013.

[31] W. Youn and S. A. Gadsden, "Combined quaternion-based error state Kalman filtering and smooth variable structure filtering for robust attitude estimation," *IEEE Access*, vol. 7, pp. 48989–14900, 2019.

[32] R. V. Vitali, R. S. McGinnis, and N. C. Perkins, "Robust error-state Kalman filter for estimating IMU orientation," *IEEE Sensors Journal*, vol. 21, pp. 3561–3569, Feb. 2021.

[33] Z. Dai and L. Jing, "Lightweight extended Kalman filter for MARG sensors attitude estimation," *IEEE Sensors Journal*, vol. 21, no. 13, pp. 14749–14758, 2021.

[34] J. K. Lee, E. J. Park, and S. N. Robinovitch, "Estimation of attitude and external acceleration using inertial sensor measurement during various dynamic conditions," *IEEE Trans. Instrum. Meas*, vol. 61, pp. 2262–2273, August 2012.

[35] P. J. Escamilla-Ambrosio, "Attitude estimation using a neuro-fuzzy tuning based adaptive Kalman filter," *Journal of Intelligent and Fuzzy Systems*, vol. 29, pp. 479–488, 10 2015.

[36] C. W. Kang and C. G. Park, "Attitude estimation with accelerometers and gyros using fuzzy tuned Kalman filter," in *2009 European Control Conference (ECC)*, pp. 3713–3718, August 2009.

[37] S. Park, J. Park, and C. G. Park, "Adaptive attitude estimation for low-cost MEMS IMU using ellipsoidal method," *in IEEE Transactions on Instrumentation and Measurement*, vol. 69, pp. 7082–7091, September 2020.

[38] K. Li, L. Chang, and B. Hu, "Unscented attitude estimator based on dual attitude representations," *IEEE Trans. Instrum. Meas*, vol. 64, pp. 3564–3576, December 2015.

[39] C. Hajiyev and H. E. Soken, *Fault tolerant attitude estimation for small satellites*. Boca Raton: CRC Press, 2020.

[40] H. E. Soken and C. Hajiyev, *Fault Tolerant Estimation of UAV Dynamics via Robust Adaptive Kalman Filter*. In Complex Systems,Bern: Springer, London/Berlin pp.369-394, 2016.

[41] C. Hajiyev and H. E. Soken, "Robust adaptive Kalman filter for estimation of UAV dynamics in the presence of sensor/actuator faults," *Aerosp. Sci. Technol.*, vol. 28, pp. 376–383, July 2013.

[42] B. Candan and H. E. Soken, "Estimation of attitude using robust adaptive Kalman filter," in *2021 IEEE 8th International Workshop on Metrology for AeroSpace (MetroAeroSpace)*, pp. 159–163, 2021.

[43] B. Candan and H. E. Soken, "Robust attitude estimation using IMU-only measurements," *IEEE Transactions on Instrumentation and Measurement*, vol. 70, pp. 1–9, 2021.

[44] A. L. Majdik, C. Till, and D. Scaramuzza, "The Zurich urban micro aerial vehicle dataset," *The International Journal of Robotics Research*, vol. 36, no. 3, pp. 269–273, 2017.

[45] M. Burri, J. Nikolic, P. Gohl, T. Schneider, J. Rehder, S. Omari, M. W. Achtelik, and R. Siegwart, "The EuRoC micro aerial vehicle datasets," *The International Journal of Robotics Research*, vol. 35, no. 10, pp. 1157–1163, 2016.

[46] H. E. Soken and S. ichiro Sakai, "Attitude estimation and magnetometer calibration using reconfigurable TRIAD+filtering approach," *Aerospace Science and Technology*, vol. 99, p. 105754, 2020.

[47] D. Gebre-Egziabher, G. H. Elkaim, J. D. Powell, and B. W. Parkinson, "Calibration of strapdown magnetometers in magnetic field domain," *Journal of Aerospace Engineering*, vol. 19, no. 2, pp. 87–102, 2006.

[48] H. E. Soken, "A survey of calibration algorithms for small satellite magnetometers," *Measurement*, vol. 122, pp. 417–423, 2018.

[49] M. D. Shuster, “Survey of attitude representations,” *Journal of the Astronautical Sciences*, vol. 41, pp. 439–517, Oct. 1993.

[50] L. Euler, “Formulae generales pro translatione quacunque corporum rigidorum, "general formulas for the translation of arbitrary rigid bodies"," *Novi Commentarii academiae scientiarum Petropolitanae*, vol. 20, pp. 189–207, 1776.

[51] J. B. Kuipers, *Quaternions and Rotation Sequences: A Primer with Applications to Orbits, Aerospace and Virtual Reality*. Princeton University Press, 2020.

[52] P. Groves, *Principles of GNSS, Inertial, and Multisensor Integrated Navigation Systems, Second Edition*. 2013.

[53] J. J. Gray, “Olinde Rodrigues’ paper of 1840 on transformation groups,” *Archive for History of Exact Sciences*, vol. 21, no. 4, pp. 375–385, 1980.

[54] R. M. Murray, S. S. Sastry, and L. Zexiang, *A Mathematical Introduction to Robotic Manipulation*. USA: CRC Press, Inc., 1st ed., 1994.

[55] W. Rowan Hamilton, “On a new species of imaginary quantities connected with a theory of quaternions,” in *Proceedings of the Royal Irish Academy*, vol. 2, pp. 424 – 434, Dublin, 1844.

[56] H. Goldstein, *Classical Mechanics*. Addison-Wesley, 1980.

[57] P. Singla, D. Mortari, and J. Junkins, “How to avoid singularity when using Euler angles?,” *Advances in the Astronautical Sciences*, vol. 119, pp. 1409–1426, January 2005.

[58] M. D. Shuster, “The QUEST for better attitudes,” *Journal of the Astronautical Sciences*, vol. 54, pp. 657–683, Dec. 2006.

[59] L. F. Markley and J. Crassidis, *Fundamentals of Spacecraft Attitude Determination and Control*. Springer-Verlag New York, 2014.

[60] H. D. Black, “Early development of transit, the navy navigation satellite system,” *Journal of Guidance, Control, and Dynamics*, vol. 13, no. 4, pp. 577–585, 1990.

[61] L. F. Markley and D. Mortari, "Quaternion attitude estimation using vector observations," *Journal of The Astronautical Sciences*, vol. 48, pp. 359–380, 2000.

[62] J. R. Wertz, *Spacecraft attitude determination and control*, vol. 73. Springer Netherlands, 1978.

[63] M. D. Shuster, "Approximate algorithms for fast optimal attitude computation," in *Guidance and Control Conference*, 1978.

[64] Cilden Guler, Demet and Hajiyev, Chingiz, "Singular value decomposition based satellite attitude determination using different sensor configurations," *Int. J. Metrol. Qual. Eng.*, vol. 8, p. 15, 2017.

[65] D. Mortari, "ESOQ: A closed-form solution to the Wahba problem," *Journal of The Astronautical Sciences*, vol. 45, pp. 195–204, 1997.

[66] L. Markley, "Attitude determination from vector observations: A fast optimal matrix algorithm," *Journal of the Astronautical Sciences*, vol. 41, 07 1993.

[67] J. Wu, Z. Zhou, J. Chen, H. Fourati, and R. Li, "Fast complementary filter for attitude estimation using low-cost MARG sensors," *IEEE Sensors Journal*, vol. 16, no. 18, pp. 6997–7007, 2016.

[68] N. J. Sanket, "Mahony filter." `https://nitinjsanket.github.io/tutorials/attitudeest/mahony.html`. Accessed: 23/08/2021.

[69] N. J. Sanket, "Madgwick filter." `https://nitinjsanket.github.io/tutorials/attitudeest/madgwick.html`. Accessed: 23/08/2021.

[70] M. S. Grewal and A. P. Andrews, *Kalman Filtering: Theory and Practice with MATLAB*. Wiley-IEEE Press, 4th ed., 2014.

[71] T. Harada, H. Uchino, T. Mori, and T. Sato, "Portable absolute orientation estimation device with wireless network under accelerated situation," in *IEEE International Conference on Robotics and Automation*, pp. 1412–1417, 2004.

[72] S. Guo, J. Wu, Z. Wang, and J. Qian, "Novel MARG-sensor orientation estimation algorithm using fast Kalman filter," *Journal of Sensors*, May 2017.